Master's Thesis in Climate Dynamics

- Physical Oceanography -

Variations of the Ice Shelf Water in the southern Weddell Sea, Antarctica

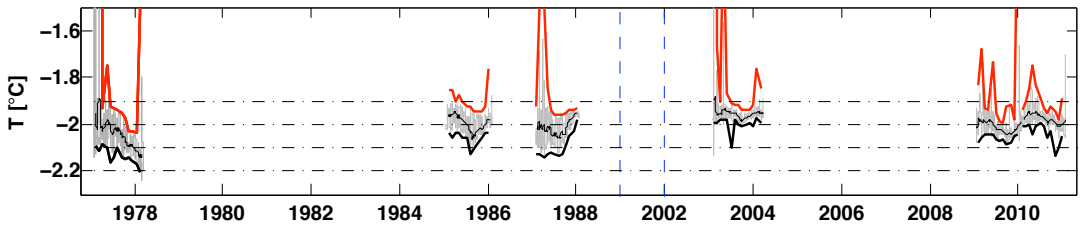

Kjersti Opstad Strand

Geophysical Institute

University of Bergen

June 6, 2011

Figure on front page shows the whole temperature series at the mooring site, S2, in the southern Weddell Sea. Note that the data from 2010 are from a Microcat, while the other series are from RCM. The figure is made in Matlab R2009b.

Acknowledgements

First I would like to thank my supervisor, Svein Østerhus for all the guidance, discussions and, not least, the valuable experiences I have gained through the trips with him; meeting other scientists around the world in Bremenhaven, Germany, letting me have an oral talk in Rosendal, a poster at the EGU meeting in Vienna, Austria, and most importantly, the scientific cruise to the Weddell Sea, Antarctica, collecting data and just getting the chance to meet penguins, encounter icebergs and to get a glance at the vast Antarctic Ice Sheet. It then comes naturally to thank Captain John Marshall and his crew on RRS Ernest Shackleton for the successful and safe encounter with the harsh Antarctic waters. I would also like to thank my co-supervisor, Elin Darelius for the constructive and helpful feedbacks, my fellow students and friends through five years for all the good times, and my mom and dad for always being supportive in what I do. Finally, I would like to thank all the tough and clever Norwegian scientists that have, through great efforts and difficult cruises, collected this unique data set, and especially Tor Gammelsrød who in 2009 presented this wonderful opportunity a bright spring day at UNIS, Svalbard.

Abstract

Ice Shelf Water (ISW) characteristics are investigated using data from moored instruments in the southern Weddell Sea. Most attention is given to the temperature data, but additional current, salinity and oxygen data are included to increase the credibility of the observations. The main data set is from a mooring site, named S2, located at the Filchner Sill. Year-long time series exists in 1977, 1985, 1987, 2003 and 2010 making this one of the longest time series in Antarctic waters. To supplement the S2 series, data are included from the FR1 mooring, southeast of the S2 position. Both seasonal and interannual variability are observed in the ISW at the Filchner Sill. Any long-term trend in the ISW is not found. A new explanation of the seasonal signal is presented, suggesting that the signal is a result from the forcing in front of the Ronne Ice Shelf. Changes in atmospheric forcing, the occurrence of polynyas and grounded icebergs are suggested to be the reason for interannual variations.

Contents

1

Introduction

The large-scale ocean circulation is mainly driven by winds and density differences between water masses, and influenced by Earth's rotation and the geometry of basins. The vertical circulation is largely determined by water-density differences and is therefore often referred to as the Global Thermohaline Circulation (GTHC). This circulation plays an important role in; bringing oxygen-rich surface waters to the bottom, ventilating the deep ocean, bringing nutrient-rich bottom water to the surface, increasing the biological production in the surface layers and transporting heat towards the poles.

The bottom water originating from Antarctica, defined as Antarctic Bottom Water (AABW), occupies large portions of the deep ocean (Gill, 1973). It is the densest water mass in the world's oceans because of the low temperature (e.g. (Foldvik & Gammelsrød, 1988; Fahrbach *et al.* , 2004)). AABW is therefore an important component in the climate system. Understanding its formation may help us understand temporal variations of the global ocean circulation and possible responses to a changing climate (Nicholls *et al.* , 2009; Carmack, 1990). One source location of AABW is the Weddell Sea (Brennecke & Seewarte, 1921; Foldvik & Gammelsrød, 1988), which is the location of focus in this study. The source water of AABW originating from the Weddell Sea is the cold, oxygen-rich and relative low-salinity Weddell Sea Bottom Water (WSBW) (Foldvik & Gammelsrød, 1988; Foldvik *et al.* , 2004).

The low temperature and salinity of the WSBW is due to the contribution of Ice Shelf Water (ISW), which obtain its final characteristics by sea ice formation over the continental shelf of the southwestern Weddell Sea and the circulation underneath the ice shelf (Foldvik & Gammelsrød, 1988; Nicholls *et al.* , 2001;

Foldvik *et al.* , 2001). The ISW flowing out of the ice shelf cavity eventually ends up in the abyss of the Weddell Sea (Foldvik *et al.* , 1985a, 2004; Nicholls *et al.* , 2009). Any changes to the ISW production, properties and/or quantity might result in changes of the AABW. An increased understanding of variability within the ISW may therefore help us understand the sensitivity of the AABW in the deep ocean (Foldvik *et al.* , 2004). The properties of the ISW plume is the result of air-ice-ocean interactions, and monitoring this plume over a long period may in addition help us understand the variability of such interactions and their role in the climate system (Nicholls *et al.* , 2009).

The purpose of this study is to examine variations of the ISW formed in the southern Weddell Sea. The main data being used are data from the long-term monitoring mooring site, named S2, located at the Filchner Sill in the south-western Weddell Sea, Antarctica (figure 2.1). This particular location is chosen because the ISW flow over the Sill when escaping the Filchner Depression (Foldvik *et al.* , 1985a). ISW mixes with off-shelf water masses at the continental shelf slope and contributes to the formation of AABW (Foldvik *et al.* , 2004).

The first S2 mooring was deployed in 1977, and the site was reoccupied in 1985, 1987, 2003, 2009 and 2010. All moorings gave at least one year of data, making this one of the longest time series in Antarctic waters. To supplement the S2 series, data are included from the FR1 mooring, southeast of the S2 position. Additional data used are CTD (Conductivity Temperature Depth) profiles taken in the same time period around the S2 mooring site. The primary focus will be on temperature data.

The S2 mooring in 2009 had sensors for dissolved oxygen, giving the very first year-long time series of oxygen in the southern Weddell Sea. An overview and a first look into this unique data set is presented here.

2

Oceanographic Setting

2.1 The Southern Ocean

The Southern Ocean is defined as the ocean between the Antarctic continent and the Subtropical Convergence (at approx. 40-50°S). It is the only zonal ocean in the world linking the Atlantic, Pacific and Indian Ocean together. The lack of meridional barriers leads to a zonal wind system forcing the ocean surface.

The mean atmospheric features over the Southern Ocean are cyclonic (clockwise) circulations (low pressure areas). The easterly winds blowing off the continent drives the westward Polar Current (East Wind Drift), while the westerly winds drive the eastward flowing Antarctic Circumpolar Current (ACC). Since the Ekman transport is to the left of the wind in the southern hemisphere, the sea-surface in the region of the ACC slopes down towards the Antarctic continent generating a geostrophic slope current to the east (the same direction as the wind) extending the ACC to great depths (Colling, 2001). This current's main obstacle is the Drake Passage located between the South American continent and the Antarctic Peninsula. The transport through this somehow narrow passage has been calculated to be 134 Sv (Nowlin Jr. & Klinck, 1986), which indicates that the ACC is the most powerful current in the world. There are four basins around Antarctica; the Weddell Basin, the South Indian Basin, the Southwest Pacific Basin and the Southeast Pacific Basin(Carmack, 1990), where the one of interest here is the Weddell Basin.

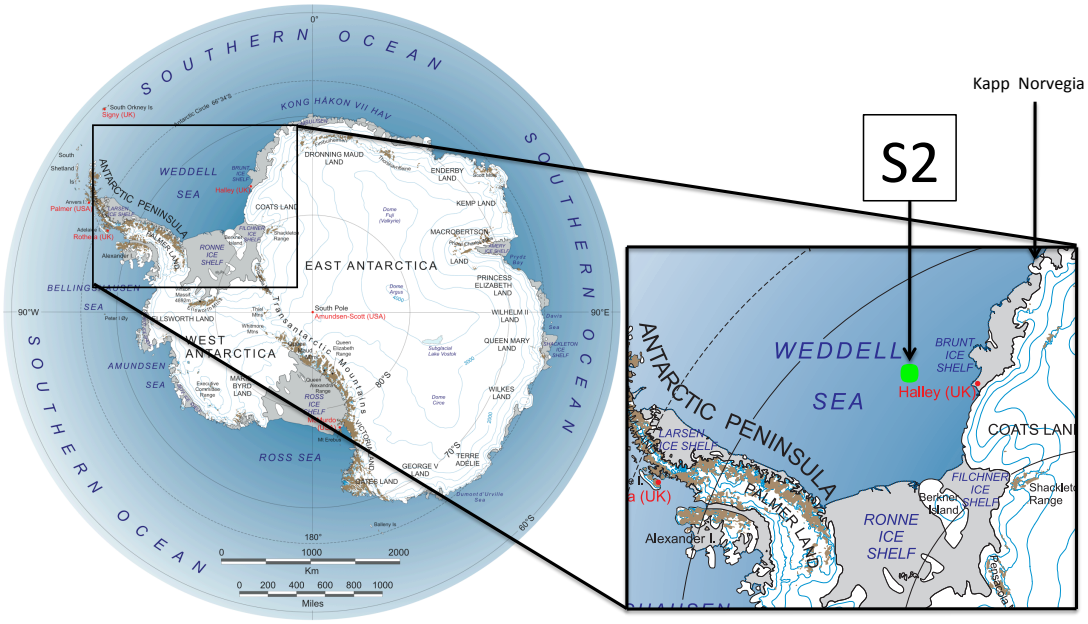

Figure 2.1: An overview of Antarctica. The map is taken from www.lima.usgs.gov/. Location of the S2 mooring is shown.

2.2 The Weddell Sea

The Weddell Sea is the most southern part of the Atlantic Ocean, from the Antarctic Peninsula in the west to Kapp Norvegia in the east (figure 2.1). The Weddell Basin has depths exceeding 5000 m with wide continental shelves (figure 2.2). The Antarctic Ice Sheet slowly moves out from the continent and floats on the sea over large areas (Foldvik & Gammelsrød, 1988). The floating glacial ice is defined as an ice shelf.

The dominant glacial feature in the Weddell Sea is the Filchner-Ronne Ice Shelf (FRIS) located in the southwestern Weddell Sea. The FRIS is the largest of the Antarctic ice shelves (by ice volume), with an area of 450,000 km^2 and an average thickness of around 700 m (Lambrecht *et al.* , 2007). The vast, relatively shallow continental shelves are downsloping towards the Antarctic continent creating a cavity underneath the ice shelf.

As in the rest of the Southern Ocean, the mean atmospheric pressure system in the Weddell Sea is cyclonic resulting in the clockwise circulation of the subpolar Weddell Gyre and an area of divergence and hence upwelling in the center.

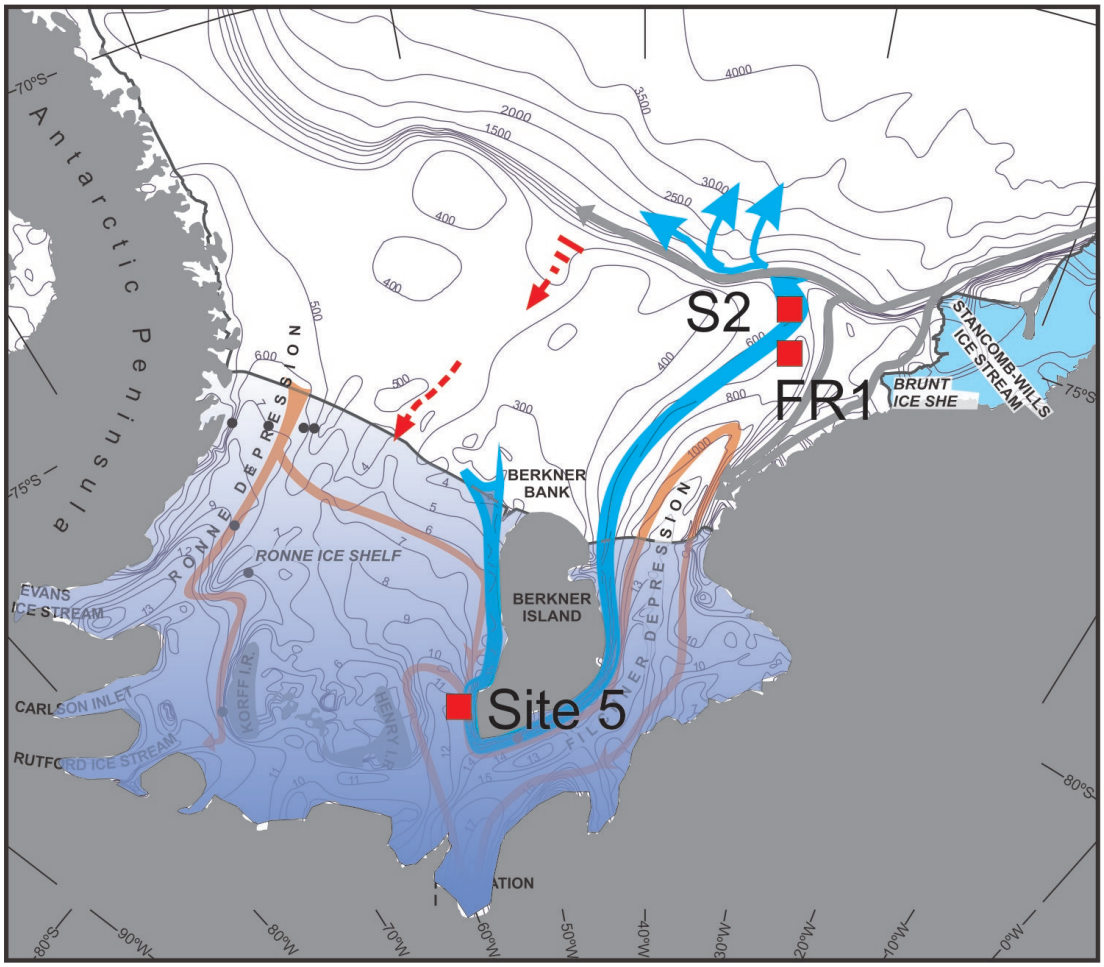

Figure 2.2: The circulation beneath the Filchner-Ronne Ice Shelf. The figure is adapted from Nicholls *et al.* (2009). Blue and red arrows show the circulation beneath the ice shelf of waters originating from the eastern and western ends of the Ronne Ice Front, respectively. The thick red broken arrow indicates the location of an MWDW inflow at the central trough in the Ronne continental shelf break. The locations of the moorings under investigation (S2, FR1 and Site 5) are labeled.

There are two depressions in the bottom topography underneath the Filchner-Ronne Ice Shelf: The Filchner Depression in the east and the Ronne Depression in the west (see figure 2.2). These depressions partly trap the heavy water formed underneath the ice shelves. The Filchner Depression extends from underneath the Filchner Ice Shelf and northward towards the continental shelf break where it is bounded by the Filchner Sill with a depth of $\sim$ 600 m (Foldvik *et al.* , 1985a; Nicholls *et al.* , 2009). The Ronne Depression is a smaller feature not extending far north from the ice front, and the circulation regimes between these two locations are therefore not completely comparable (Nicholls *et al.* , 2003). This study will mainly be concerned with the cyclonic circulation (Carmack & Foster, 1975b) in the Filchner Depression. The circulation over the southwestern continental shelf and underneath the FRIS is shown in figure 2.2 together with the location of the instruments under investigation.

The coldest and the densest deep water mass in the world originates from the Weddell Sea. The reason for such a water mass production is the combination of the large floating Filchner-Ronne Ice Shelf and the favourable topography in form of a downsloping continental shelf with depressions. How this heavy water is formed and its relation to the floating FRIS is described in details in section 2.3.2.

2.3 Water masses in the Southern Ocean

Water masses are traditionally defined from a general temperature/salinity classification (see figure 2.3), and the Southern Ocean is no exception. A summary of the water masses are given in table 2.1. The definitions of the water masses are taken from Carmack (1990) and Foldvik *et al.* (1985d).

The surface layers (upper 50 to 200 m) north of the continental slope contain Antarctic Surface Water (AASW), a cold and relatively fresh water mass which has obtained its characteristics from upwelled deep water modified by surface exchange processes. Below this water mass there is a temperature minimum layer with slightly higher salinities, called Winter Water (WW). This water mass evolve during wintertime when AASW is cooled to the surface freezing point and brine is added to the water column due to ice formation. Within the Antarctic Circumpolar Current a relatively nutrient-rich water mass originating from North Atlantic Deep Water (NADW) called Circumpolar Deep Water (CDW) is found

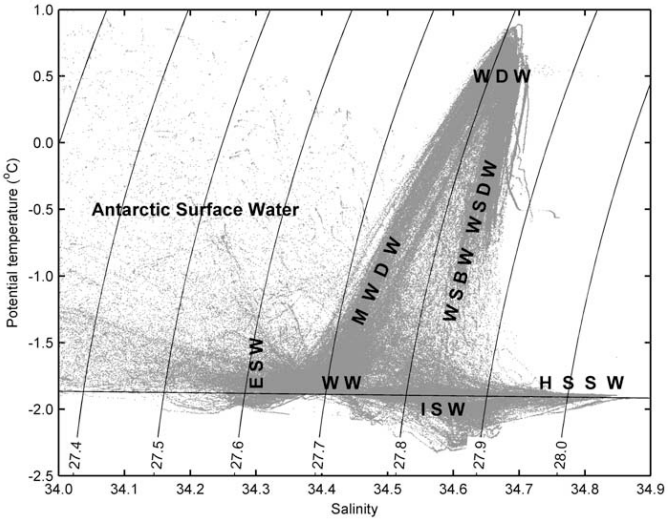

Figure 2.3: A θ-S diagram showing the water masses in the Weddell Sea south of 70°S. The isopycnals are calculated with respect to surface pressure and the straight line is the surface freezing temperature. The figure is taken from Nicholls *et al.* (2009).

Table 2.1: Overview of the main water masses on the Southern Weddell Sea Shelf. The definitions of the water masses are taken from Carmack (1990) and Foldvik *et al.* (1985d)

AABW	Antarctic Bottom Water	$-0.7 < \theta < 0.0°C$ $34.64 < S < 34.68$
AASW	Antarctic Surface Water	$S < 34.3$
CDW	Circumpolar Deep Water	$\theta > -0.5°C$
HSSW	High-Salinity Shelf Water (Western Shelf Water)	$\theta \sim -1.9°C$ $S > 34.70$
ISW	Ice Shelf Water	$\theta < -1.9°C$
LSSW	Low-Salinity Shelf Water (Eastern Shelf Water)	$\theta \sim -1.9°C$ $34.28 < S < 34.44$
MWDW	Modified Warm Deep Water	$\theta \sim -1.2°C$ $S \sim 34.5$
WDW	Warm Deep Water	$0 < \theta < 0.8°C$ $34.64 < S < 34.72$
WSBW	Weddell Sea Bottom Water	$\theta < -0.7°C$ $S \sim 34.65$
WW	Winter Water	$\theta \sim -1.9°C$ $34.28 < S < 34.52$

at intermediate depths. A cooler and fresher variety of CDW extending southward is the Warm Deep Water (WDW). At the ocean floor Weddell Sea Bottom Water (WSBW) is found. A thorough description of WSBW will be given in section 2.3.1.

Over the continental shelf there is more variability in the water column. During summertime a relative warm and fresh seasonal layer is formed from radiative heating and ice melting. Below this there is either High-Salinity Shelf Water (HSSW) or Low-Salinity Self Water (LSSW) depending if you are located more to the west or to the east of the Filchner Depression, respectively. These water masses have temperatures near the surface freezing point and covers most of the shelf floor. HSSW has salinity close to the threshold salinity for driving deep convection and is therefore an important part of the deep water formation. LSSW has slightly lower salinity, but is still an important mixing component in AABW (Jacobs *et al.* , 1985). A mixture of WDW and WW is called Modified Warm Deep Water (MWDW) and is identified as a warm intrusion. This is an almost continuous feature, but it tends to break up into parts when mixed with ambient shelf waters at its most southern part (Foster & Carmack, 1976). There are found cores of Ice Shelf Water (ISW) in both the Ronne and the Filchner Depression. This water mass is defined as waters with temperatures below the surface freezing point ($\sim< -1.9^\circ$ C). ISW is a result of the cooling at the base of the ice shelves due to the depression of freezing temperature with increasing pressure. A more detailed explanation of this water mass is given in section 2.3.2.

Compared with the rest of the continental shelf, the hydrography over the Filchner Sill is slightly different. An ISW plume is flowing over the Sill from the Filchner Depression and down the continental slope (Foldvik *et al.* , 1985a). An illustration of the water mass distribution over the Filchner Sill is shown in figure 2.4.

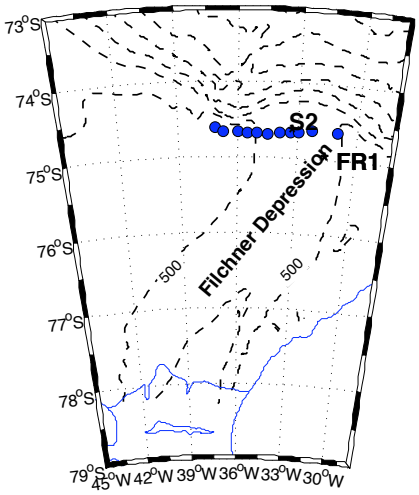

(a) Map over CTD section

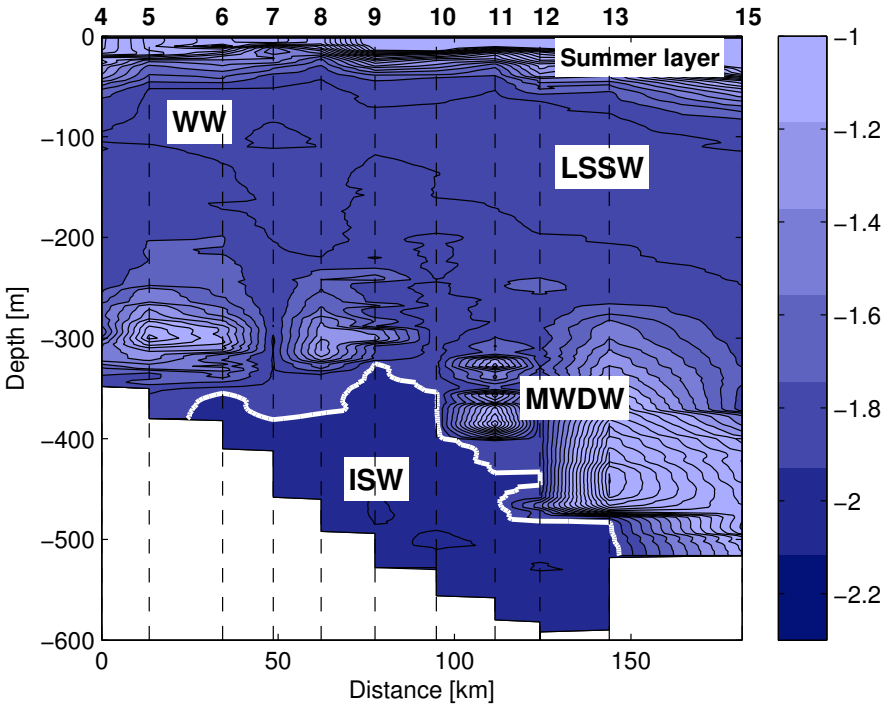

(b) Water masses over the Filchner Sill

Figure 2.4: An overview of the hydrography over the Filchner Sill. a) Map of the section over the Filchner Sill. Note that the section is west-east oriented. b) The temperature section across the Filchner Sill from the Norwegian Antarctic Research Expedition (NARE) cruise in 1985. The thick white line marks the −1.9° C isotherm. The water mass definitions is adapted from Grosfeld *et al.* (2001). The stations with its respective labels are marked with dashed lines.

2.3.1 Deep water in the Weddell Sea

Research on bottom water has traditionally been on the mechanisms that produces deep water, and what locations are the most effective producers. There have been found two types of Weddell Sea Bottom Water (WSBW). Gill (1973) presented how Western Shelf Water (WSW) is formed (now called HSSW) when brine releases into the water column due to ice formation. This water mixes with MWDW and WDW along the continental shelf break (frontal mixing), eventually sinking down the continental slope forming WSBW (Nicholls *et al.* , 2009). The second type of WSBW is formed by mixing between ISW and the overlying WDW (Foldvik *et al.* , 1985a,d). This latter process is one of the results obtained from the Norwegian Antarctic Research Expeditions (NARE) to the Southern Weddell Sea in the time period 1976-1985 (Foldvik & Gammelsrød, 1988). Foldvik *et al.* (2004) estimated the rate of WSBW formation by the ISW plume over the Filchner Sill to be 4.3 ± 1.4 Sv. A third mechanism of deep water formation proposed by Gordon (1998), is the direct flow of HSSW down the continental slope.

2.3.2 Ice Shelf Water

The ISW plume at the Filchner Sill was detected during the Norwegian Antarctic Research Expedition 1976/1977 (Foldvik *et al.* , 1985a). Using all available current meter records from the same region, Foldvik *et al.* (2004) found that 1.6 ± 0.5 Sv of ISW passes Filchner Sill

During the freezing season the water on the shallow continental shelves is cooled to the freezing point of seawater ($\sim -1.9°C$), then ice starts to form resulting in a salinity increase of the water below and formation of HSSW. Some of this water flows into the deeper parts of the ice shelf cavity where the local freezing point is lower than the surface freezing point. The freezing point decreases with increasing depth (pressure) (see section 3.3). Because the glacial ice has a temperature of between -20 and $-25°C$, the water flowing into the cavity is warming the ice shelf by heat conduction through the ice, and the circulating water is henced cooled. When the ice shelf base has reached the in-situ freezing point, ice starts to melt, diluting the circulating water (and cooling it further). The fresher water will be buoyant and rise. The local freezing point will then increase, leading to formation of frazil ice at the ice base. There will therefore be a small temperature increase because of the latent heat released when freezing occur. The whole process is often referred to as an "ice pump" (Grosfeld *et al.* , 2001). A schematic

illustration is shown in figure 2.5. The resulting water mass formed by these processes is ISW, reaching temperatures lower than $-2.0°C$ (Lusquiños, 1963). ISW is colder than the surface freezing point and is therefore often referred to as supercooled. This water which contain meltwater from the ice shelf flows out of the ice shelf cavity and over the continental shelf break. Here it mixes with WDW creating WSBW, which eventually transform into WSDW.

Ice production is large in front of the Filchner-Ronne Barriers (because of tides and off-shore winds maintaining areas of open water (Foldvik *et al.* , 2001)), and dense water is therefore located in these areas. Due to gravity some of this water will flow southward into the cavity of the Ronne Ice Shelf (Nicholls & Østerhus, 2004). The waters circulates underneath the ice shelf around Berkner island eventually ending up at the western side of the Filchner Depression (Foldvik & Gammelsrød, 1988), see figure 2.2. During the passage under the ice shelf the transformation from HSSW to ISW occurs. The inflow of HSSW into the ice shelf cavity is strongly seasonal due to the seasonality in the sea ice formation (Nicholls, 1996). During the winter the water column is homogeneous due to mixing. The ice shelf draft limit the water movement according to the Taylor-Proudman theorem (Nicholls *et al.* , 2009), see section 3.4. During summer, the meltwater is decoupling the water and the water can flow beneath the ice shelf due to gravity. An additional, but smaller scale, inflow occur both winter and summer because of tidal motions (Makinson & Nicholls, 1999). There have been detected two inflow regimes of HSSW; one from the Berkner Bank (Foldvik *et al.* , 2001) and one from the Ronne Depression (Nicholls *et al.* , 2003).

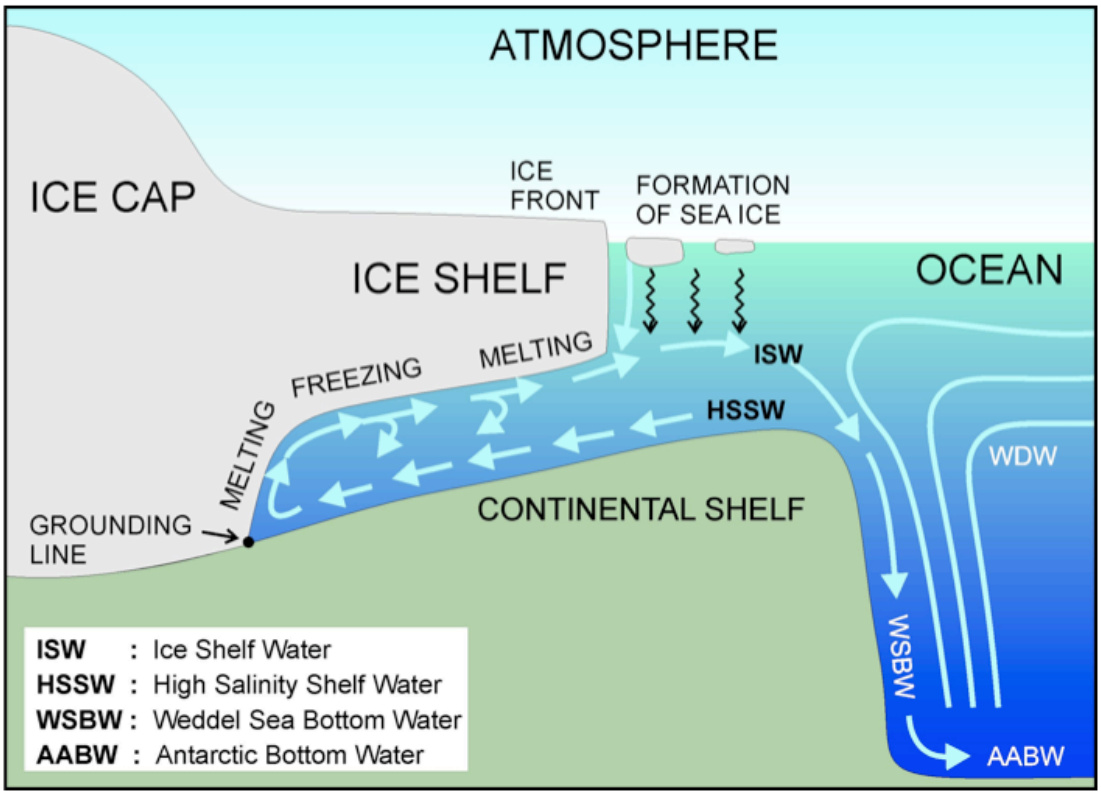

Figure 2.5: A simple schematic illustration of the formation of Ice Shelf Water underneath the floating ice shelves (courtesy to the Geophysical Institute, UIB).

2.4 Ice Cover

The ice cover mainly consist of sea ice and large pieces of ice broken off the floating ice shelves, called icebergs. During the winter, after the sea-surface has cooled to its freezing point, ice starts to form. Much of the pack ice in Antarctica either melts during the summer or drift northward in the Weddell Gyre. Most parts of the pack ice is therefore first-year ice (Foldvik & Gammelsrød, 1988). The seasonality of the ice extent is illustrated in figure 2.6.

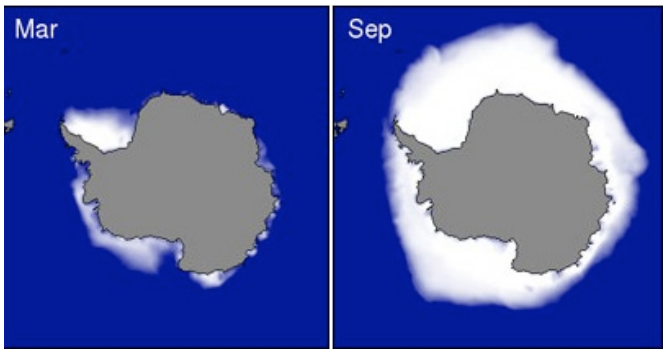

Figure 2.6: Ice cover around Antarctica, in March (Austral autumn) and September (Austral spring). The illustration is taken from www.nsidc.org/sotc.

There are local fluctuations in the ice production due to the occurance of open water areas (polynyas and leads) within the ice cover.

A polynya is an extensive area of open water. There are two types of polynyas; open-ocean polynyas and coastal polynyas. Open-ocean polynyas (or sensible heat polynyas) develop away from land where the heat loss is compensated by heat from below, preventing ice formation. Coastal polynyas (or latent heat polynyas) are formed by tidal forcing or when winds blow the ice away from the Antarctic continent. The ice is transported away creating a zone of open water where new ice can form resulting in high local sea ice production. The salt drained out during the freezing process is left in the water column increasing the density of the water.

Leads are smaller features formed by diverging or shearing ice drift induced by wind and/or tidal forcing. They are shaped like narrow, linear cracks in the sea ice.

3

Physical properties of seawater

3.1 Density of seawater

The density of seawater depends on its temperature, salinity and pressure (depth). The density increases with decreasing temperature, increasing salinity and/or increasing depth. The dependence of density on temperature and salinity is non-linear. For example the density is less sensitive to temperature changes at low temperatures than at high temperatures (Pond & Pickard, 2003).

Temperature
The energy of the water molecules decreases with decreasing temperatures and the tendency of the water molecules to arrange in ordered groups increases. The effect of decreased temperature is therefore increased density.

Salinity
Salt molecules have a higher mass than water molecules, thus adding dissolved salts into the water increases the density. In addition, the salinity increases the ability of water molecules to arrange themselves, increasing the density further.

Pressure - Compressibility of seawater
The density of seawater increases with increasing depth due to the compressibility of seawater. Because the ability of water molecules to form ordered groups is greater at low temperatures, cold water is more compressible than warm water. Thus, the density dependence on temperature increases with increasing pressure. This is called *thermobaricity*.

Maximum density at atmospheric pressure

Freshwater has its density maximum close to $4°C$ at atmospheric pressure, but with increasing salinity, the temperature of maximum density decreases. This is because the dissolved salts prevent the tendency of water molecules to form in ordered groups and thermal expansion is the only controlling effect on density (Brown & Bearman, 1999), i.e. saltwater is able to reach a lower temperature before ice starts to form, and thus a higher density. For salinities higher than about 25, the maximum density of seawater correspond to the freezing point (Brown & Bearman, 1999).

3.2 Adiabatic temperature changes

Adiabatic temperature changes are those that occur without any heat transfer from ambient waters. A water parcel exposed to higher pressure is compressed gaining internal energy and thereby increasing its temperature. It is therefore important to distinguish between *in-situ* temperature T, and *potential* temperature θ when considering the stability of the water column. In-situ temperature is the temperature of the fluid measured at its actual depth, while potential temperature is the temperature a fluid would have if brought adiabatically up to the sea surface. When using potential temperature the compressibility effect is eliminated. Since the data used in this thesis are compared at their respective depths, the in-situ temperature will be used, otherwise it will be stated in the text.

3.3 The freezing point of seawater

The freezing point temperature is dependent on salinity and pressure. Freshwater has its freezing point at 0°C, and by increasing the salinity the freezing point decreases. The freezing point also decreases with increasing pressure (~ -0.75°C/km (Fofonoff & Millard, 1983)). This physical behavior of the freezing point is what makes the basis for the ISW formation. The formula for calculating the freezing point is given by equation 3.1 (Fofonoff & Millard, 1983) and is shown to illustrate the behavior of the freezing temperature of seawater.

$$T_f = a_0 * S + a_1 * \sqrt{S} + a_2 * S^2 + b * P \tag{3.1}$$

where $a_0 = -0.0575$, $a_1 = 1.710523e^{-1}$, $a_2 = -2.154996e^{-4}$ and $b = -7.53e^{-4}$

For general purposes the freezing point of seawater is set to $-1.9°C$ at atmospheric pressure. The freezing temperatures in the salinity range of what is found on the continental shelf (table 3.1) confirm that this approximation is valid in this thesis.

Table 3.1: Freezing point temperatures (T_f) at the sea surface for different salinities (S). The salinities chosen are in the range of what is found on the shelf in front of the Filchner-Ronne Ice Shelf.

Surface pressure				
S	34.5	34.6	34.7	34.8
Tf	-1.8932	-1.8989	-1.9046	-1.9104

3.4 Taylor-Proudman Theorem

For a geostrophic current and a homogeneous water column, the horizontal velocity has no vertical shear;

$$\frac{\delta u}{\delta z} = \frac{\delta v}{\delta z} = 0 \tag{3.2}$$

This vertical rigidity is known as the Taylor-Proudman Theorem (Cushman-Roisin & Beckers, 2009), and states that all movement have to flow parallel to the isobaths. The ice shelf front can be thought of as a step in the topography for the flow of waters because the draft is large relative to the water depth.

4

Instruments and Methods

The primary measurements used in this thesis are from instruments at the mooring site, S2, in the southern Weddell Sea (at the Filchner Sill), Antarctica (figure 4.1). Moored instruments have been deployed during cruises in the years 1977, 1985, 1987, 2003, 2009 and 2010, giving a time series longer than 30 years (admittedly with substantial gaps). The particular placement is chosen because the Ice Shelf Water (ISW) flow over the Sill when escaping the Filchner Depression [Foldvik et al., 1985a].

The moorings were equipped with Aanderaa Instruments Recording Current meters (models RCM4, RCM7 and RCM9) (www.aadi.no). In 2009 a new bottom mounted system for long-term monitoring (more than 5 years), the BIAC system (www.bccr.no/biac), was deployed at S2. The mooring deployed in 2010 contained Sea-Bird Electronics Microcats (SBE-37) (www.seabird.com) in addition to RCM instruments. Table A.1 gives an overview of the instruments at the S2 site. Note that the S2 mooring in 2009 is bottom moored (at depth of 602 m), but will be compared with the instruments at 25 m above bottom (m.a.b) for the other years. Additional data used are from CTD (Conductivity Temperature Depth) profiles from cruises around the S2 position during the time period from 1977 until 2010. The CTD instruments have varied in time from the types Neil Brown and Falmouth Scientific Inc (FSI) to SeaBird Electronics (SBE). See appendix A for a more thorough description of the moored instruments and the CTD instruments.

All RCM instruments were equipped with sensors for measuring current speed, direction, temperature and, in some cases, a conductivity cell for salinity measurements. Factory calibrations have been used for the speeds and directions,

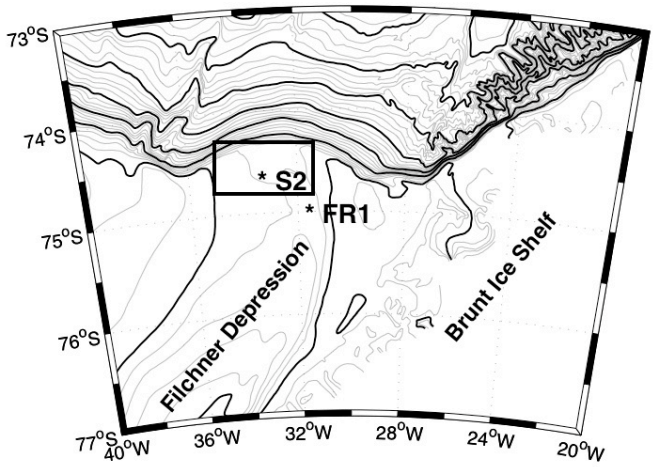

(a) Southern Weddell Sea

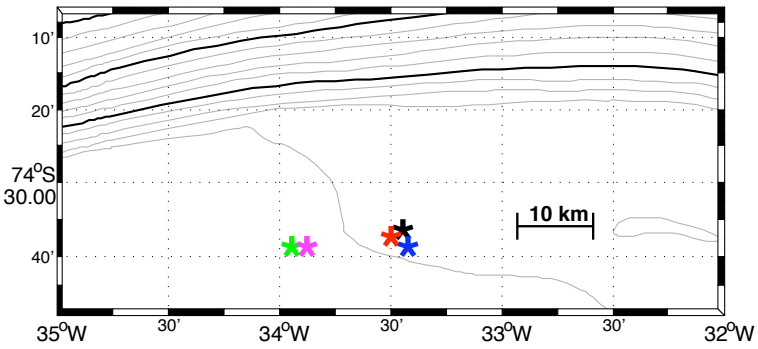

(b) S2 positions

Figure 4.1: a) The southern Weddell Sea with the locations of the S2 and FR1 moorings. The black square is the zoomed area in b) showing the change of placement of the S2 mooring from year to year. b) The S2 position in 1977 and 1985 (magneta), 1987 (green), 2003 (blue), 2009 (red) and 2010 (black) with local topography from GEBCO bathymetry data (www.gebco.net).

Table 4.1: Overview of the long-term S2 moorings and the instruments used in this thesis. Columns indicate deployment year, latitude, longitude, instrument type, bottom depth, the depth of the instruments given in meters above bottom (m.a.b.) and number of days with recorded data. Note that the S2 moorings in 1985 and 2010 are the only ones containing RCM in three levels.

S2 moorings						
Year	**Lat.**	**Lon.**	**Type**	**B. Depth [m]**	**m.a.b.**	Rec. Days
1977	-74 40	-33 56	RCM 4	558	100	257
			RCM 4		25	411
1985	-74 40	-33 56	RCM 4	545	190	258
			RCM 4		100	283
			RCM 4		25	371
1987	-74 40	-34 00	RCM 7	558	100	404
			RCM 7		25	352
2003	-74 40	-33 28	(Broken)	597	153	-
			RCM 9		102	747
			RCM 9		27	421
2009	-74 39	-33 33	RCM 9 IW	602	0	365
			RDCP 602		0	356
2010	-74 38	-33 30	RCM 7	612	176	182
			RCM 7		104	364
			SBE-37		26	364
			RCM 7		25	364

and the accuracy of the individual measurements are ± 1 cms^{-1} and $\pm 5°$, respectively (Foldvik *et al.* , 2004). Systematic errors might occur at low speeds due to mechanical resistance in the rotors (Savonious or paddle rotor), but this is not a concern here. The compass readings are corrected for magnetic deviations of $+4°$. Factory calibrations for the temperature sensors give an accuracy better than 0.05°C (Foldvik *et al.* , 2004). In-situ calibration of the temperatures have been carried out with CTD (see appendix B). All, except the 1977 deployment, gave temperature variance within the sensor accuracy. The instruments in 1977 have not been factory calibrated nor lab calibrated, so the data have been corrected against the in-situ CTD temperature (see appendix B). Wrong calibration of the temperature series at 25 m.a.b for the S2 mooring in 1987 have previously been used[1]. See appendix B for comparison between the two calibrations (Wide range calibration was used instead of an Arctic range). The only conductivity data included are from 2009, where there exist two conductivity sensors, which were checked against each other, see appendix C. In general, the RCM's conductivity sensors need to be in-situ calibrated to obtain accurate salinity values. Due to their inaccuracy, the salinity data have not been given much attention.

[1]wrong calibration for the RCM at 25 m.a.b at S2 was used in the article by Foldvik *et al.* (2004).

The BIAC system (deployed in 2009) is equipped with an AADI 600 kHz Recording Doppler Current Profiler (RDCP 600) in addition to a modified RCM9 equipped with sensors for temperature, conductivity and dissolved oxygen (Optode). Only one temperature sensor recorded successfully, but there are two independently data sets for both dissolved oxygen and conductivity (see figure C.6 and C.7). Factory calibrations are used for all these sensors. The accuracy of the dissolved oxygen Optode is $< \pm\mu$M or $\pm 5\%$ (www.aadi.no). The conductivity sensor has an initial accuracy of 0.0018 S/m, but unfortunately the AADI sensor suffers from drift and therefore need to be in-situ calibrated against CTD (pers. com. Østerhus). Due to problems with the downloading of the RDCP current data, these are not included.

The 2010 mooring contained three RCM7s and three[2] SBE-37 (with an initial accuracy of 0.002°C (SeaBird Electronics, 2011)) allowing for comparison between instruments calibrated at two independent factories (see appendix C). This has been done for the temperature, and the difference was inside RCM7's accuracy (< 0.04°C), see figure 4.2 (and figure C.4). The difference is in accordance to the findings by Foldvik *et al.* (2004).

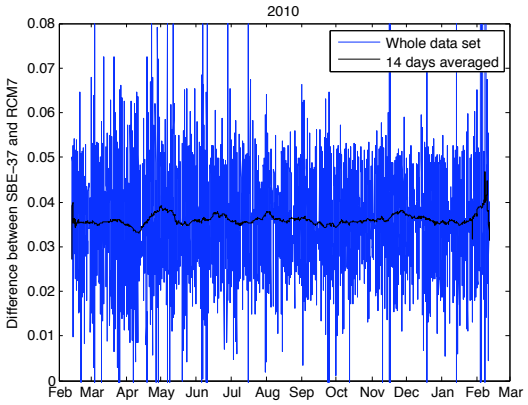

Figure 4.2: Difference between SBE-37 and RCM7 in 2010. The SBE-37 (Microcat) is placed 26 m above bottom (m.a.b), while the RCM7 is located 25 m.a.b.

To fill the gap in the S2 temperature series, data have been included from the FR1 mooring, located southeast of the S2 location in the time period from 1995 to 1997 (see figure 4.1 and appendix A for lat./lon. positions). The calibration procedure has been carried out by the Alfred-Wegener-Institute (Østerhus, pers.

[2]only the deepest Microcat is presented here.

com.) and previously used by Foldvik *et al.* (2004). The ISW plume path passes FR1 before it reaches the S2 (see figure 2.2). The depth of the deepest RCM instrument at FR1 (590 m) is comparable to the depth of the deepest instrument at S2, and more importantly, it is placed above the sill level (of $\sim$ 600m (Foldvik *et al.* , 1985a)). The water masses measured at the deepest instrument at FR1 (20 m.a.b.) are therefore likely to pass the lowest instrument at S2.

The analysis of the data have been done using Matlab R2009b for Mac OS X. The same is the case for all the figures. The time series are low-pass filtered using a 7th. order Butterworth design with cut-offs specified in the text. In some cases running means are used giving the best graphical presentation. In those cases, seven days are cut-off from the ends of each time series to remove the energy transferred to the end parts. Months with less than 15 days of recorded data have not been included when calculating monthly means.

4.1 Calibration and data credibility

This data set (at S2) contain six year-long time series spread over 33 years. Can these narrow windows reveal the truth about the variations of the ISW plume flowing over the Filchner Sill? To answer this question it is important to understand the limitations of the sensors, recording systems and the data-processing tools.

It is important to remember the uncertainty of the sensors when investigating the small temperature variations in this thesis. Data from several types of instruments with different sensors and accuracies have been analyzed. The temperature sensors at the RCM are less accurate than the sensors on the CTD, so cross-calibrating with different instruments give higher confidence in the data. Two independent sensors measured conductivity and dissolved oxygen in 2009, and both a RCM and a Microcat measured temperature in 2010 allowing comparisons to be done. Several types of filtering methods are used giving the same results, increasing the credibility of the observations. The sample duration are long enough to investigate seasonal cycles and interannual variability. With the established theory and earlier analyses in the Antarctic, there is in addition confidence to discuss long-term trends.

5

Results

Data from instruments at the long-term mooring site, S2, and CTD sections occupied in the same area, are presented. Temperature data from the FR1 mooring in 1995 southeast of S2 (figure 4.1(a)) are included to supplement the data series from S2.

In table 5.1 the annual means of temperature and velocity with its standard deviations from the S2 moorings are listed. Yearly mean potential temperatures at the deepest RCM instruments are below -2.00°C, except in 2003 when it is -1.97°C. The lowest mean temperature at S2 occurs in 1977, when the temperature is ~ 0.1°C lower than the other years. The upper instrument in 1987 is the only instrument, other than the deepest ones, that has a mean potential temperature lower than $-2.00°$. The standard deviations of temperature are smallest at the deepest instruments, and increases with decreasing depth. The u-component of the current is always directed westward. The v-component is directed northward, except at the shallowest instrument in 2010 where it is slightly southward. The yearly mean current speeds are quite similar in magnitude at all available levels for the different years, except in 2003 where the shallowest instrument measures a slow mean current speed compared to the other instruments. The deepest instruments in 2003 and 2010 measures higher current speeds than pre-2003.

Table 5.1: Summary of annual means from the S2 current meter moorings with its respective standard deviations (u is positive eastward and v is positive northward). NI stands for "not included" data. Lines illustrate non-exisitng values. In addition the values used from the FR1 mooring are listed.

Yearly means on S2 with corresponding standard deviations											
Depl. Year	Obs. Depth [m]	Mab [m]	Rec. Days	θ [°C]	ϕ_θ [°C]	u [cm s^{-1}]	ϕ_u [cm s^{-1}]	v [cm s^{-1}]	ϕ_v [cm s^{-1}]	sp [cm s^{-1}]	ϕ_{sp} [cm s^{-1}]
1977	458	100	257	-1.93	0.34	-6.1	11.0	4.3	10.0	14.4	8.3
	533	25	411	-2.15	0.15	-5.7	8.9	5.4	8.3	12.7	6.9
1985	355	190	258	-1.66	0.31	-3.6	9.9	2.4	10.2	13.18	6.8
	445	100	283	-1.96	0.17	-3.7	9.9	4.1	10.4	13.20	7.8
	520	25	371	-2.01	0.05	-4.8	9.4	6.0	9.6	13.6	7.4
1987	459	100	404	-2.02	0.17	-6.2	11.1	3.5	11.7	15.8	7.7
	533	25	352	-2.03	0.06	-4.9	9.0	3.9	9.4	12.7	7.0
2003	495	102	747	-1.89	0.26	-5.2	4.3	0.9	4.5	7.5	3.1
	570	27	421	-1.97	0.10	-13.6	11.3	4.8	12.7	20.0	9.9
2009	602	0	365	-2.02	0.11	NI	NI	NI	NI	NI	NI
2010	436	176	182	-1.77	0.38	-13.4	10.6	-1.6	10.7	18.5	8.3
	508	104	364	-1.94	0.26	-15.1	10.4	1.8	11.1	19.7	8.7
	586	26	364	-1.99	0.04	-	-	-	-	-	-
	587	25	364	-2.03	0.04	-15.0	11.0	7.1	12.8	21.6	9.6
FR1											
1995	590	20	691	-2.04	0.03	NI	NI	NI	NI	NI	NI

5.1 Temperature

Figure 5.1 shows the conditions in the bottom layers at S2 in 2009, representing typical conditions at the Filchner Sill. The temperature has variability on timescales of the order of hours to a seasonal signal. Twp types of smoothing methods are shown for comparison. Temperatures are generally below surface freezing point, indicating that the bottom layers are primary occupied by ISW. During the Austral summer the temperatures are occasionally reaching higher than -1.5°C (see appendix C), from several months in 1977 (figure C.1(a)) to no warm intrusion in 1985 (figure C.1(b)). These warmer periods have temperature characteristics matching those of MWDW, and will be discussed in section 6.1.

The attention will be given to the variability with timescales longer than one month.

Figure 5.2 is showing the low-passed filtered (14 days) temperature series at 100 and 25 meters above bottom (m.a.b) (see appendix C for the unfiltered data sets). The different years are represented separately with their respective measurements at different levels. The deepest moored instruments (in most cases 25 m.a.b) are generally measuring ISW, except occasionally during Austral summer as mentioned previously. Instruments at 100 m.a.b show larger variability in the

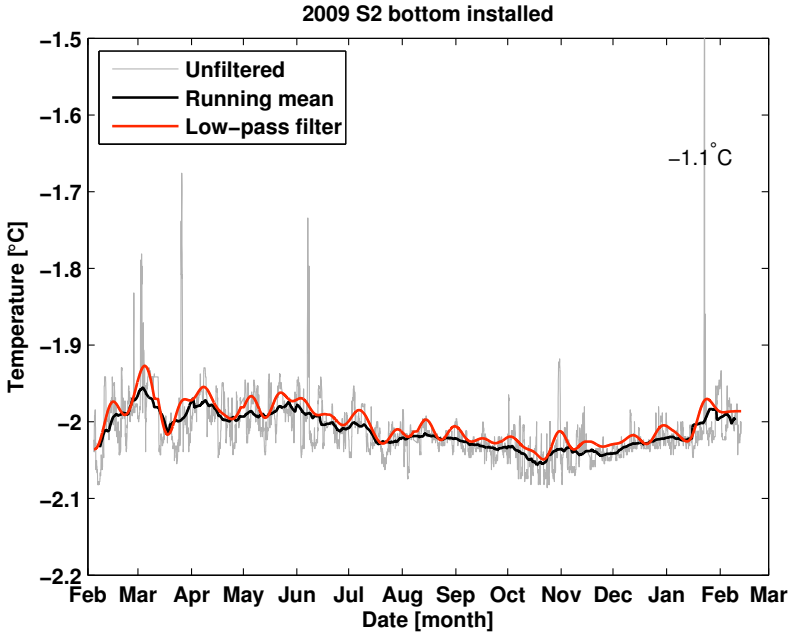

Figure 5.1: Temperature (25 m above bottom) at S2 in 2009; Unfiltered data (grey line), 14 days running mean (black line) and 14 days low-passed filtered (red line).

temperature indicating that these levels have a larger variety of water masses passing the instrument. The waters at S2 have variability with shorter timescales than one month alternating between ISW and warmer water masses (HSSW, MWDW, WW and/or ESW). The S2 moorings from 1985 and 2010 contain instruments in three levels (figure 5.3). Temperatures from all three levels illustrate that the temperature variability increases towards the surface.

Since the focus of this study is to look at the ISW, the temperature series closest to the bottom have been given the most attention. But (at least) one interesting result appear comparing the different mooring levels, occurring at the end of 1987, when the topmost instrument measures lower temperatures than the deepest instrument (figure 5.2(c)).

The whole time series of temperature data at 25 meters above bottom [1] from the S2 site is shown in figure 5.4. The tidal signal is removed using a low-passed filtering with a 30 days cut-off. This has been done to illustrate that the short-time variance within the temperature is not caused by the diurnal and semidiurnal tidal effects. The temperatures mainly varies between $-2.20°C$ to $-1.90°C$. If 1977 is not taken into account, the temperatures varies in between a

[1] this is true for all except S2 2009 which is bottom moored at 602 m depth.

range of $\sim 0.20°C$. The lowest temperatures are measured in 1977 with a different yearly behavior. The 2003 data set have temperatures closer to HSSW with less variance.

Figure 5.5 show 100 days running means for the different levels at 100 and 25 m.a.b. Seasonal signals are seen at both levels with highest temperatures during late summer and lowest temperatures during late winter. The warm phase is longer than the cold phase. At the instruments 100 m.a.b in 1977 and 2003, the summertime intrusion of warmer waters partly mask the seasonal signal (figure 5.5(a)). The coldest temperatures at 100 m.a.b is measured in 1987. At 25 m.a.b in 1977 there is no seasonal signal. The temperatures continue to drop after the other temperature series have reached their minimum (figure 5.5(b)). The temperatures at 25 m.ab in 2003 are warmer and less variable compared with the rest of the series at the same level (figures 5.2(d) and 5.5(b)). The end of the temperature series at 25 m.a.b in 1987 gets warmer than in 2003. In 2010 the summer season is much longer compared with the other years.

The mean temperature of each month with its respective standard deviations for the deepest S2 temperature series are plotted in figure 5.6. The monthly means are the most variable when the temperatures are the highest, and the least variable when the temperatures are the lowest.

Figures 5.5(b) and 5.6 represent a climatic seasonal cycle made by interpolating monthly means using fast fourier transformation (see appendix D).

Temperature frequencies are shown in figure 5.7. The data from 1977 show the largest variance and the lowest temperatures, while 2003 have the least variance and the highest temperatures. The data set from 2003 has a higher frequency at $T = -1.95°C$ than any of the other years. The temperature seem to have a normal distribution around $-2.00°C$ in 1985, 2009 and 2010, while around $-1.95°C$ in 2003 and $-2.10°C$ in 1977. There are not much waters with temperature of $-2.00°C$ in 1987. After 1987 there is less variance in the temperature and with no or little water colder than $-2.10°C$. This can possible be linked to the change in position, see figure 4.1.

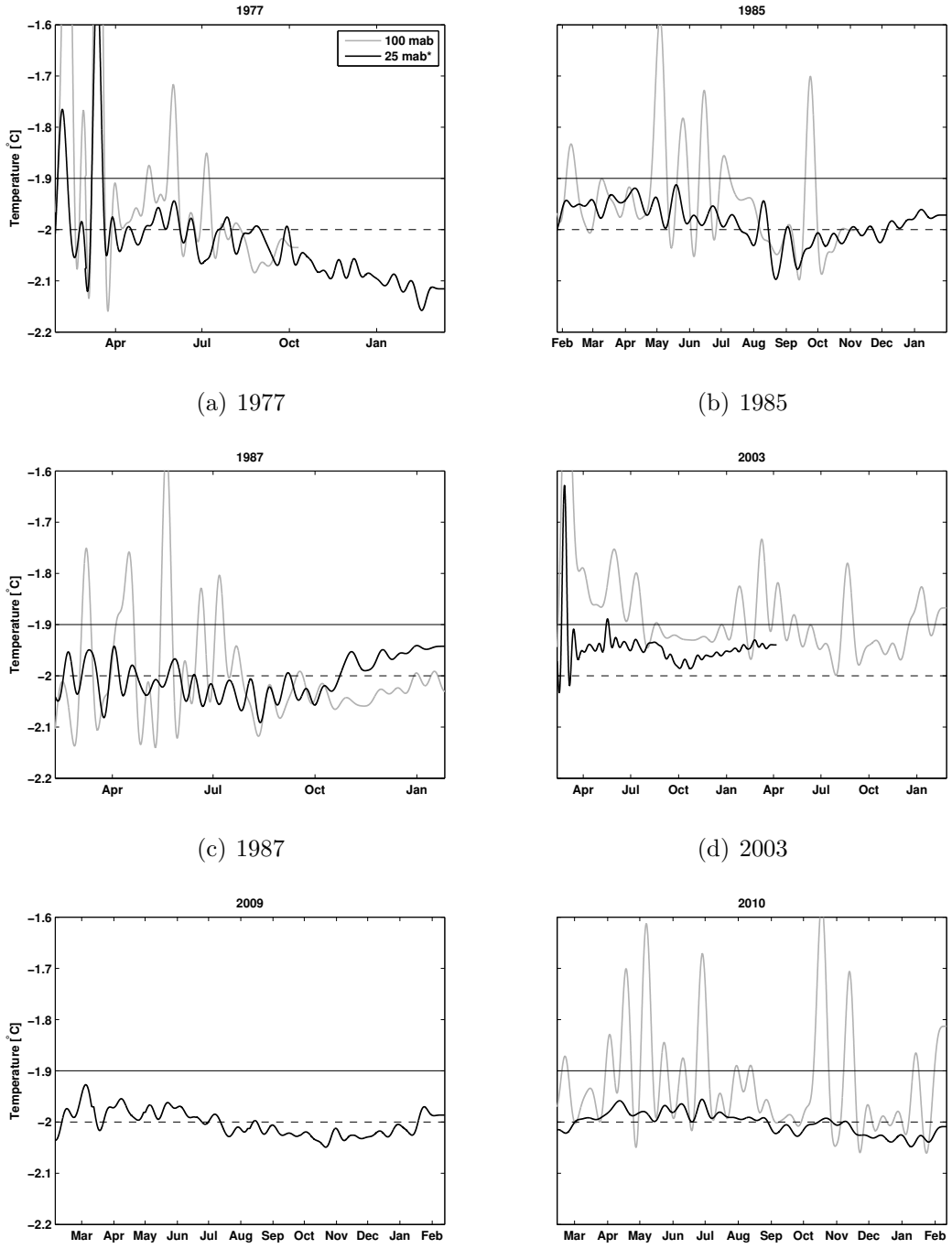

(a) 1977

(b) 1985

(c) 1987

(d) 2003

(e) 2009

(f) 2010

Figure 5.2: Current meter temperatures (two levels) at the S2 position have been low-pass filtered with a cut-off of 14 days. * S2 2009 is bottom moored at 602 m depth. The $-2.00°C$ and $-1.90°C$ isotherms are shown.

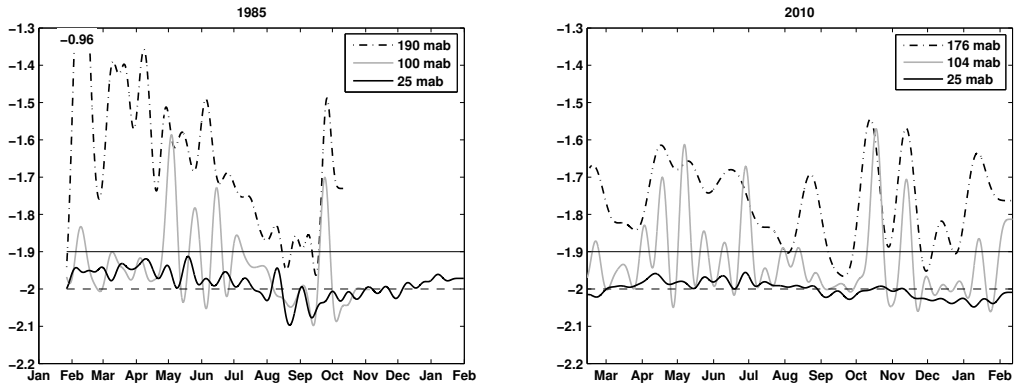

(a) 1985 All

(b) 2010 All

Figure 5.3: All 3 levels of current meter temperatures at the S2 position in 1985 and 2010. The data have been low-pass filtered with a cutoff of 14 days. The $-2.0°C$ and $-1.9°C$ isotherms are shown.

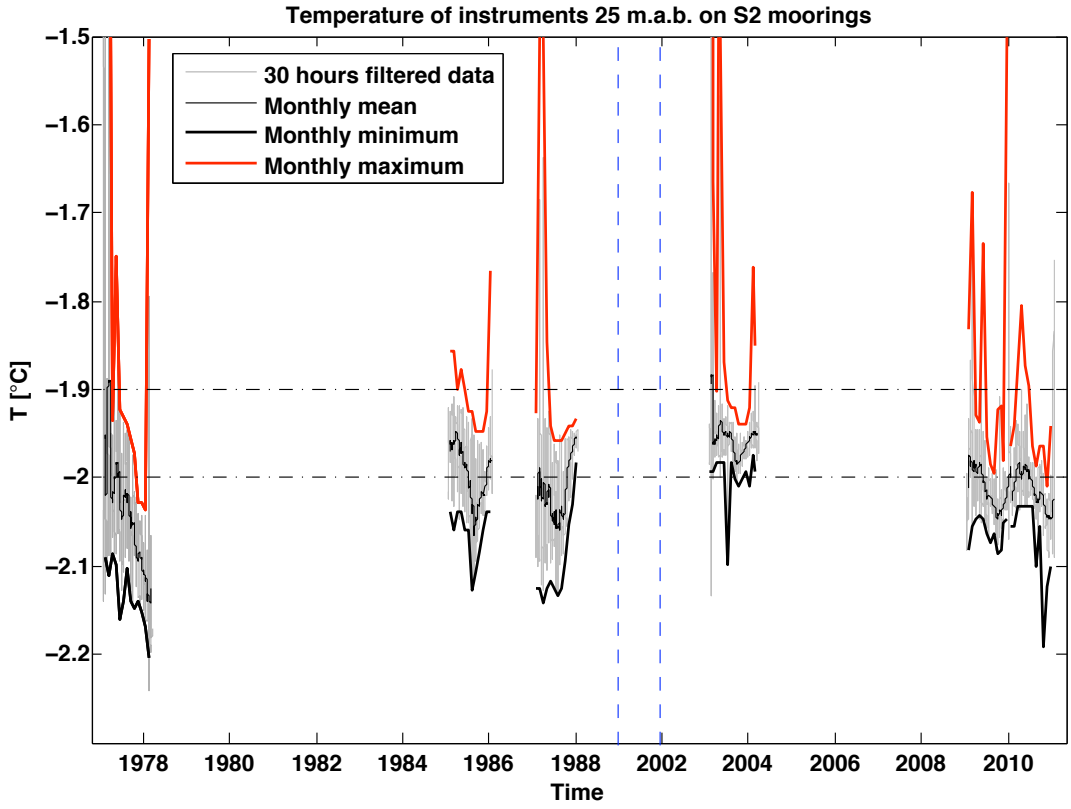

Figure 5.4: Complete temperature series 25 m.a.b at S2. The grey lines are low-pass filtered data with a cut-off of 30 hours. The thin black lines are running means over 30 days. The thick black and red lines are monthly minimums and maximums, respectively. Note that a cut-off of 12 years has been done between 1989 and 2002 marked with blue dotted lines. The dash-dotted lines show the −1.9°C and −2.0°C isotherms.

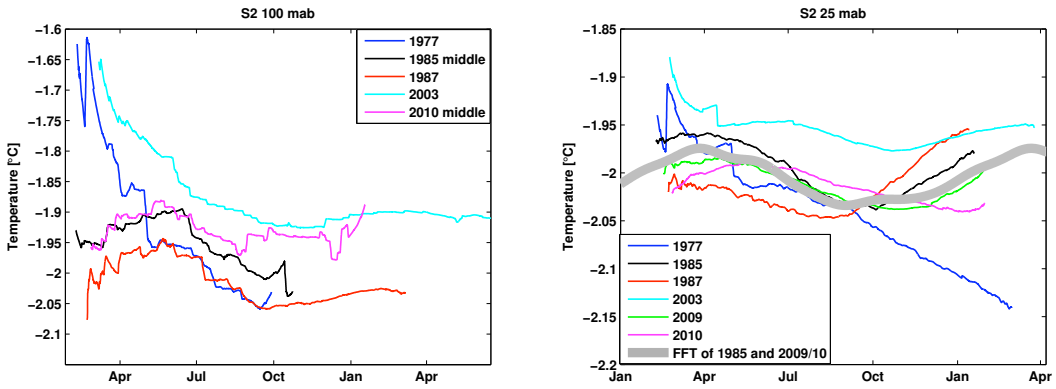

(a) 100 m above bottom.

(b) 25 m above bottom.

Figure 5.5: 100 days running mean temperature at a) 100 m.a.b and b) 25 m.a.b. Note the different scales on the y-axis. The FFT-interpolated seasonal cycle is included in figure b).

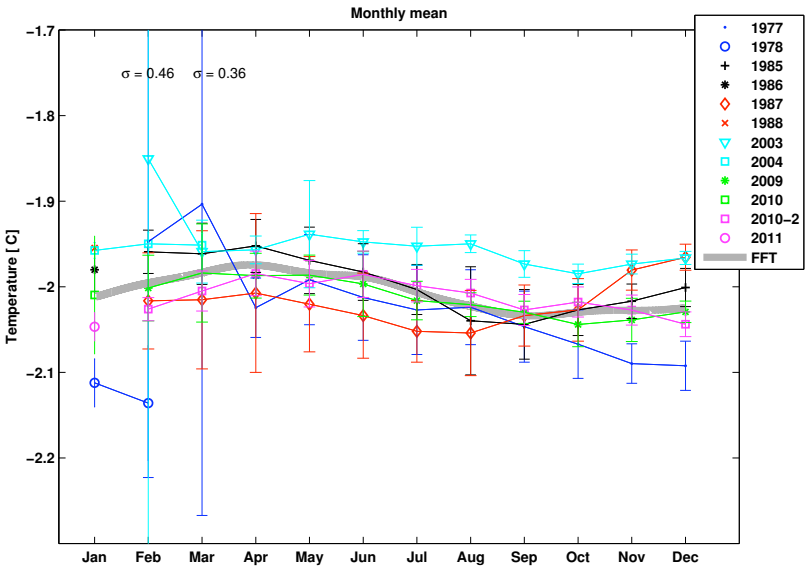

Figure 5.6: Monthly mean temperatures with standard deviations 25 m.a.b at S2. Some data from 2010 are shown both from the 2009-deployment (green square) and the 2010-deployment (pink squares). No averaging of the data sets have been done before the monthly means have been calculated.

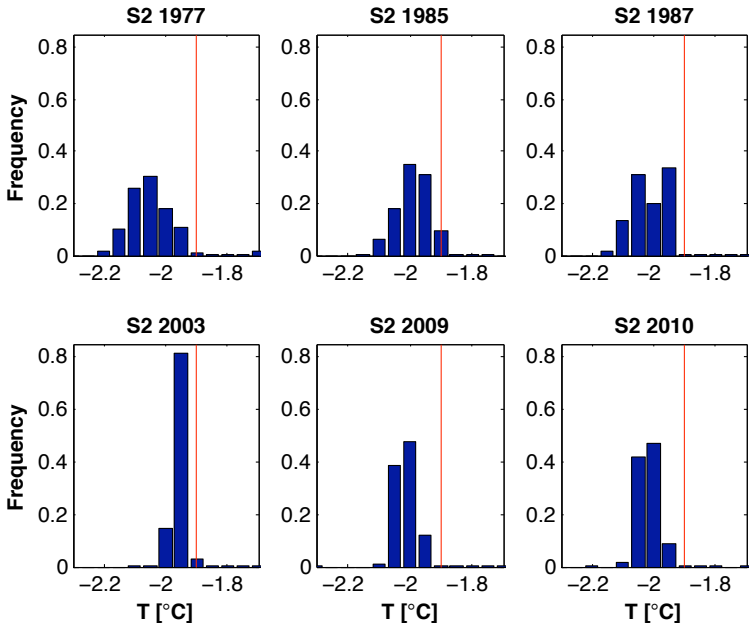

Figure 5.7: Histograms of the frequency of temperature from 25 m above bottom at S2. The temperature interval is set to be 0.05°C. The −1.90°C isotherm is shown as a red line

Seasonality

A seasonal amplitude is here defined as the difference between the highest temperature and lowest temperature during one year. The seasonal amplitude has been calculated for each year at the S2 mooring (see table 5.2) using the monthly means shown in figure 5.6. The seasonal amplitude of the interpolated seasonal cycle has been calculated to be 0.06°C (table 5.2).

Table 5.2: Seasonal amplitudes (A) defined as the different between the highest and the lowest monthly mean temperatures. The minimum and maximum temperature with its respective month is listed for each year. FFT stands for the interpolated climatic seasonal cycle.

S2			
Year	**Min. [°C] (Month)**	**Max. [°C] (Month)**	**A [°C]**
1977	No seasonal signal		-
1985	-2.04 (Sept)	-1.95 (Apr)	0.09
1987	-2.05 (Aug)	-1.96 (Dec)	0.09
2003	-1.98 (Oct)	-1.94 (May)	0.04
2009	-2.04 (Oct	-1.98 (Mar)	0.06
2010	-2.01 (Dec)	-1.95 (Jun)	0.06
Mean S2	**-2.02** **Late winter/early spring**	**-1.96** **Late summer/early fall**	**0.07**
FFT 1985,2009,2010	-2.03 (Sep)	-1.97 (Apr)	0.06

5.1.1 Including the FR1 mooring

The temperature data from FR1 is shown in figure 5.8. ISW clearly passes FR1. The temperatures are generally lower than at S2, but not as low as in 1977. The temperatures hardly reaches over $-2.00°C$ with no experiences of warm water intrusions. The yearly mean temperature (see table 5.1), however, is close to that of the bottom layers at S2. A seasonal signal is clearly seen at FR1. The temperature data have been averaged over 30 days, and the seasonal signal is found to be $0.1°C$ for both years, which is slightly higher than the calculated values at S2. This calculation of the seasonal signal differs from the method used at the S2 data to simplify the data processing.

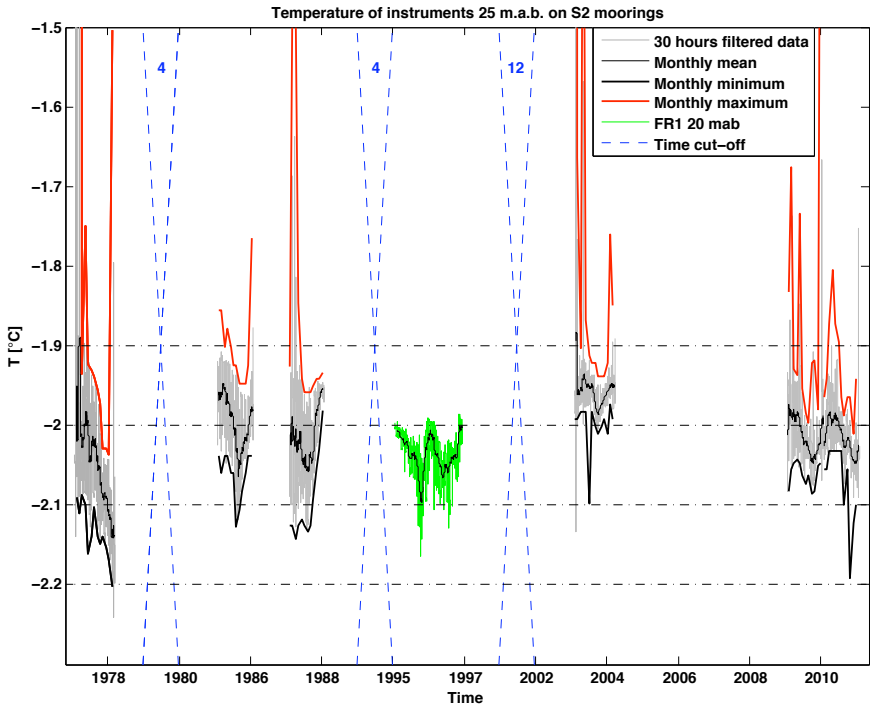

Figure 5.8: A modified version of figure 5.4 showing temperature data from S2 (grey line) and from the deepest instrument at FR1 (green line). The black line running through the data from FR1 is the 100 days running mean. The number of years cut off to make the figure more readable are labeled in the blue dash dotted crosses.

5.2 Current

In this section the current data from the S2 position are presented. The time series from the years 1977, 1985, 1987, 2003 and 2010 have been included, (current data from 2009 have not been taken into account as explained in chapter 4).

The current speeds from the deepest RCM (25 m.a.b) have been averaged over a 100 days period (figure 5.9). The years 2003 and 2010 have the highest current speeds, while the rest of the data sets exhibit similar current speeds within the range from $5 - 10$ cm/s. The higher speeds in 2003 and 2010 may occur because of the different location compared to earlier years (see figure 4.1). Seasonal signals are observed with similar phases as for the temperature data in 1985, 1987 and 2010. The lowest speeds are measured in late winter/early springs and the highest are measured during late summer/early autumn. In 2003 the curve is out of phase with the other years, i.e. the current is strongest during the summer and lowest during the autumn. A similar negative trend is seen in the current speed at the deepest instrument in 1977, as for the temperature at the same level, the same year. The linear correlations between temperature and current are found to be ~ 0.85 (1977); 0.59 (1985); 0.71 (1987); -0.53 (2003) and 0.48 (2010).

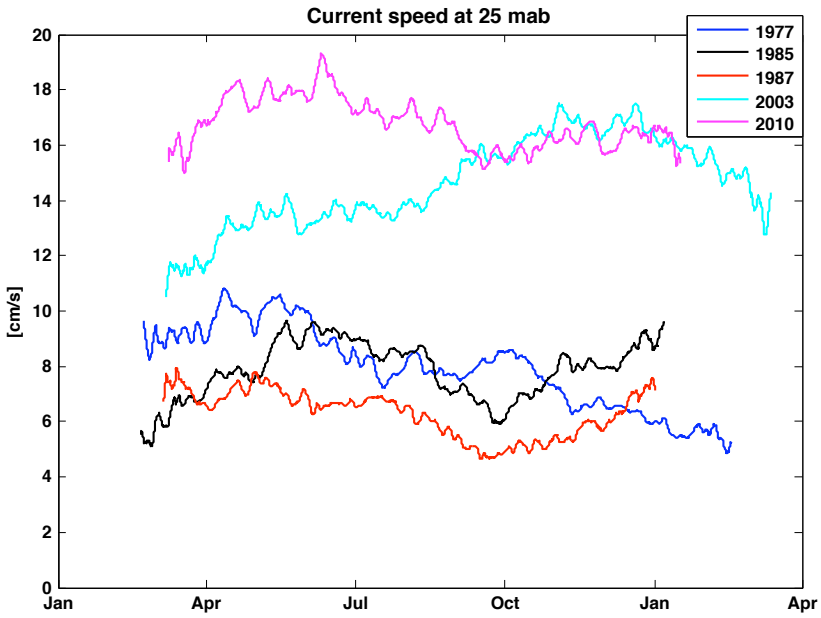

Figure 5.9: Speed (100 days running mean) at the S2 position in 1977 (blue line), 1985 (black line), 1987 (red line), 2003 (cyan line) and 2010 (magneta line).

A progressive vector diagram is shown in figure 5.10. The temperature variations of each series are shown with colors. The direction of the ISW plume is northwestward with slightly different angles from year to year. In 1987, however, the direction shifts more northward in the end of the time series. The ISW passing S2 in 2003 is warmer than the other years, faster than pervious years and has the most westward direction. In 2010 the ISW is faster than pre-2003, but the temperatures are more similar to the pre-2003 state.

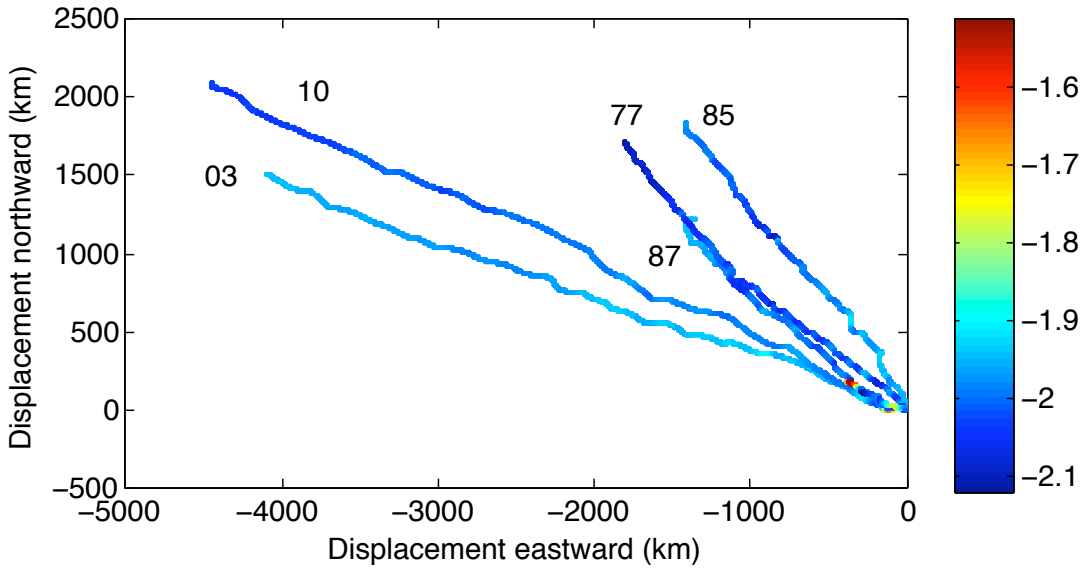

Figure 5.10: Progressive vector diagram for current data from 1977, 1985, 1987, 2003 and 2010. The time series shown are of equal length. The temporal temperature variations of each series are shown with colors. Note the change in direction towards the end of the 1987 time series.

5.3 CTD sections

Available CTD sections around the S2 position are examined. All CTD sections are occupied during Austral summer. Sections at different locations in the Filchner Depression are presented in figure 5.11. The sections were occupied in different years, and are believed to present the main climatological hydrography in the Filchner Depression. The water characteristics over the Filchner Sill have been described in chapter 2.1. The same vertical distribution of water masses are observed in the section over Filchner Sill from 1979 (figure 5.11(b)) with e.g. ISW in the bottom layers. Further south in the Filchner Depression the ISW plume is observed above HSSW (figure 5.11(c)), which has drained from the Berkner Bank (Foldvik *et al.* , 1985d). In front of the Filchner Ice Shelf there are two cores of ISW (figure 5.11(d)) representing the cyclonic circulation of ISW in the Filchner Depression (Gammelsrod & Slotsvik, 1981). The core temperature of ISW has a north-south gradient (ΔT$\sim$ 0.2°C), where it is coldest at the ice front and warmest at the Sill. Figure 5.12 show the conditions in the Filchner Depression in 2003. These sections confirm that there are warmer temperatures at the Filchner Sill and in the Depression in 2003 compared to other years investigated (as seen in the data from the S2 mooring).

Figure 5.13 shows a $\theta - S$ diagram which has been made with the available CTD data taken over the Filchner Sill from the years 1979, 1985, 1987, 1990, 1992, 1995, 1998 and 2003 (see appendix A.2 for more details). It shows that the bottom waters at the Filchner Sill in 2003 are supercooled with respect to the surface freezing point, indicating ISW characteristics even though the variance is less compared with the other years.

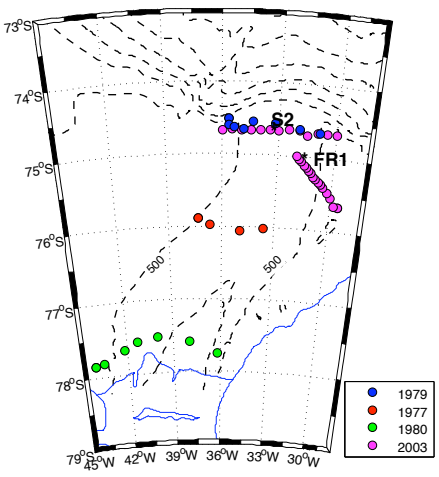

(a) Map

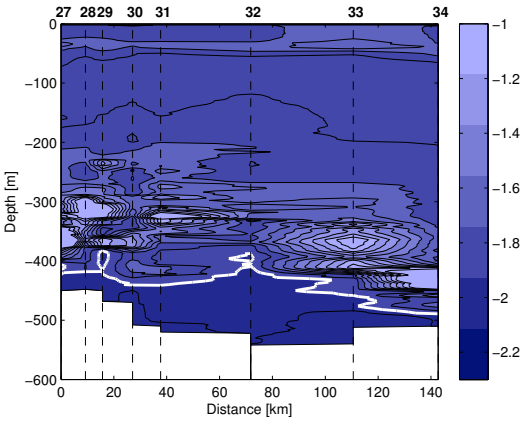

(b) Filchner Sill, 1979 (blue dots).

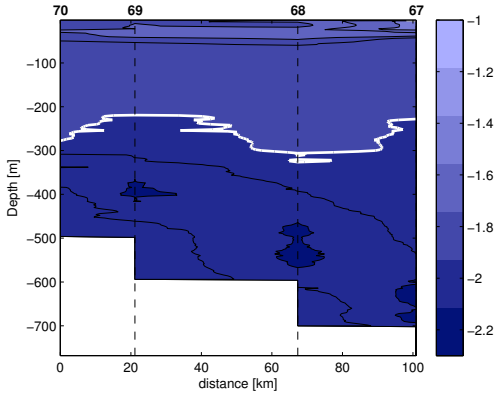

(c) Filchner Depression, 1977 (red dots).

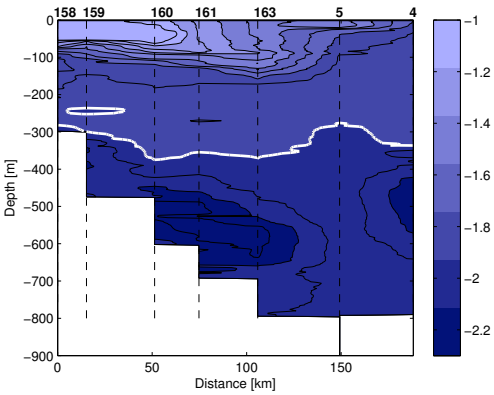

(d) Filchner Ice Front, 1980 (green dots).

Figure 5.11: a) Location of moorings S2 and FR1 and the CTD sections shown in (b-d) and fig. 5.12. Temperature sections from b) Filchner Sill, 1979 (blue dots) c) Filchner Depression, 1977 (red dots) d) Filchner Ice Front, 1980 (green dots). The thick white line marks the $-1.90°C$ isotherm, and the numbers on the top line represent each of the CTD-casts. Sections in (b-d) are all West-East oriented.

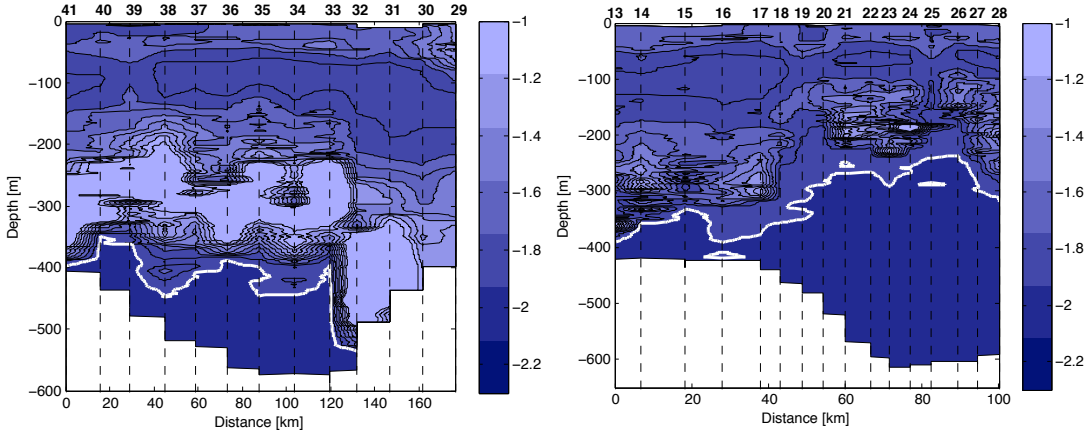

(a) Filchner Sill (b) Across Filchner Depression

Figure 5.12: Temperature sections from 2003, see figure 5.11(a) for the location (magneta dots). The thick white line marks the $-1.9°C$ isotherm, and the numbers on the top line represent each of the CTD-casts. Note that 5.12(a) is West-East oriented, while 5.12(b) is East-West oriented.

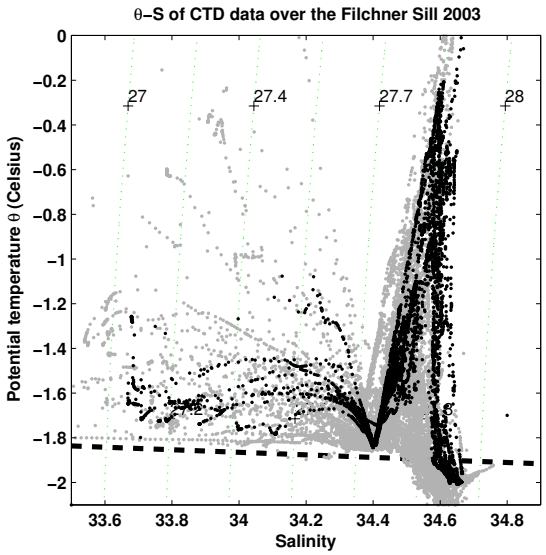

Figure 5.13: θ-S diagram of the CTD data over the Filchner Sill at pressure of 0 dbars. Note the smaller range in temperature and salinity in 2003 (black dots) compared with the other years with available data (grey dots). The dashed line represent the freezing point line.

5.4 Salinity

The salinity time series from the 2009 deployment at the S2 site are used in this analysis. During this year salinity data were available from two independently sensors at the same level (see figure C.6) showing similar signals. Since only one year of salinity data have been included in this analysis, the same type of investigations done for temperature cannot be carried out for the salinity. A brief comparison has been made between salinity and temperature.

The salinity and temperature data have been normalized and 14 days low-passed filtered for comparison (figure 5.14). From a first look the salinity data seem to have a similar seasonal signal as the temperature data (figure 5.14). A correlation between the filtered salinity and temperature is found to be 0.66.

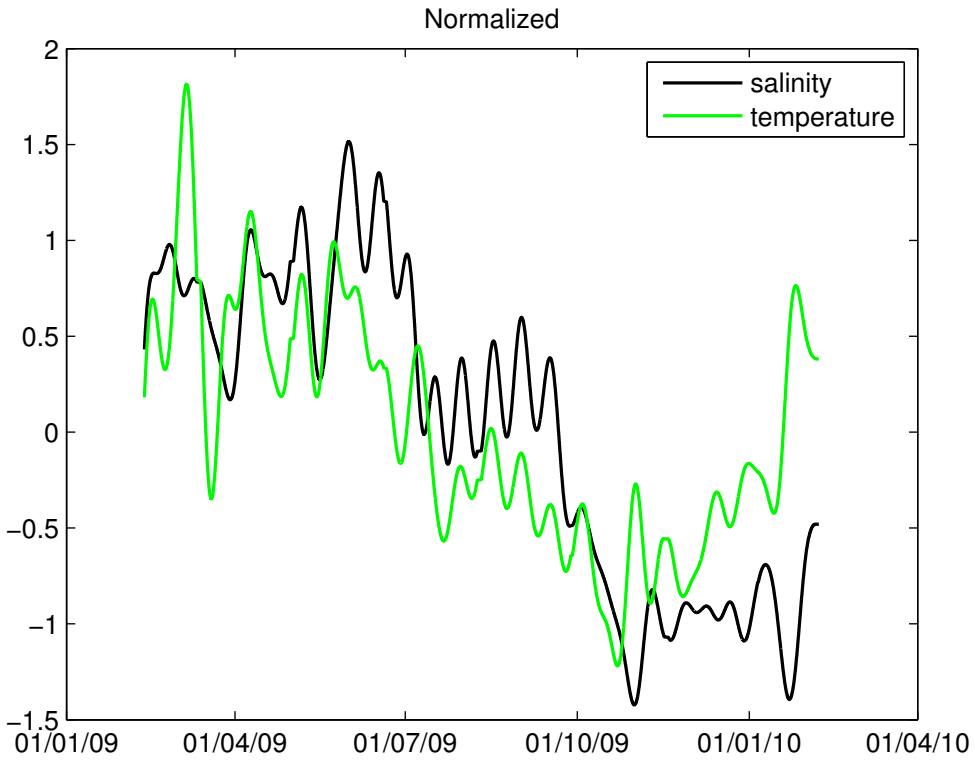

Figure 5.14: Normalized and 14 days low-passed filtered temperature and salinity data from S2, 2009.

5.5 Preliminary results of the oxygen data

The S2 mooring deployed in 2009 contained two oxygen sensors giving two independently data sets showing similar signals (see figure C.7). The sensor on the RCM is chosen because it contains a denser amount of data points. The saturation data of oxygen in seawater for the observed temperature and salinity series are shown together with the dissolved oxygen series (figure 5.15). The dissolved oxygen levels increases throughout the year, but are below saturation levels, except for one peak in mid-November 2009. The low levels in February 2010 coincides with a temperature peak (see figure 5.1) indicating MWDW.

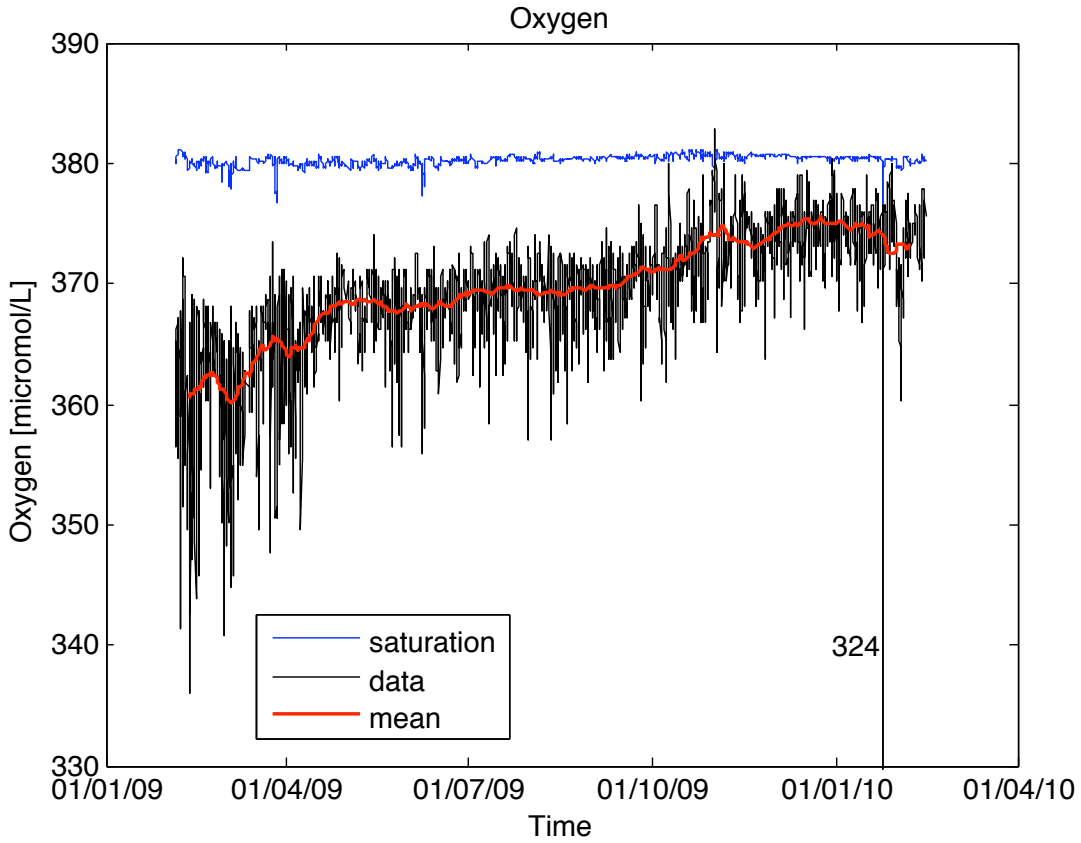

Figure 5.15: Solubility (satuaration) of Oxygen (O2) in seawater with observed temperature and salinity (blue line) and oxygen observed (black line). The data set have been averaged over a 14 days period (red line).

The different data sets (salinity and dissolved oxygen) have been normalized and 14 days low-passed filtered for comparison (figure 5.16). In addition the de-trended oxygen data are plotted in the same figure. No seasonal signal similar to the signal observed in the temperature and salinity data is observed in the oxygen data. Negative correlations are found to be ~ 0.70 between oxygen and temperature, and ~ 0.80 between oxygen and salinity in the filtered data sets. This is expected since the solubility of gases generally decreases for increasing temperature and salinity (Brown & Bearman, 1999).

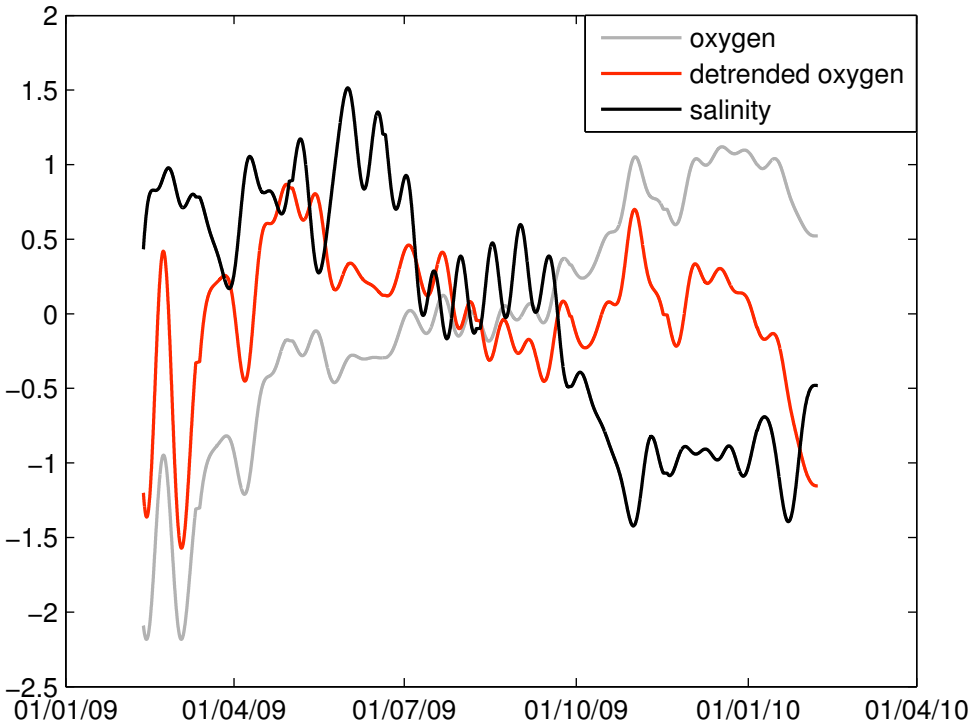

Figure 5.16: Normalized and 14 days low-passed filtered oxygen, de-trended oxygen and salinity data from S2, 2009.

6

Discussion

6.1 Warm summertime intrusion

As shown in previous chapter, the deepest instruments at S2 occasionally measured relatively warm summertime (January to April) intrusions. This water mass is identified as modified warm deep water (MWDW), which is recognized in the (summer) CTD sections taken over the Filchner Sill (see figure 2.4, 5.11 and 5.12(a)).

Figure 6.1 shows the directions when the "warm" waters are passing S2. MWDW mainly have a southwestern or western direction (i.e. they come from the northeast). In 1977 the inflowing MWDW are directed more to the south, as discussed by Foldvik *et al.* (1985c). This indicates that the inflow originates from the northeast of the Filchner Sill, which fits well with the circulation pattern of MWDW discussed by Nicholls *et al.* (2009) (see figure 6.2). This circulation is forced by winds and processes along the ice front (Nicholls *et al.* , 2009), and changes in the atmospheric forcing may be the reason for the occasional inflows of MWDW.

At FR1 there is no intrusion of MWDW supporting the observations by Foldvik *et al.* (1985d) that MWDW does not cross over the Filchner Sill.

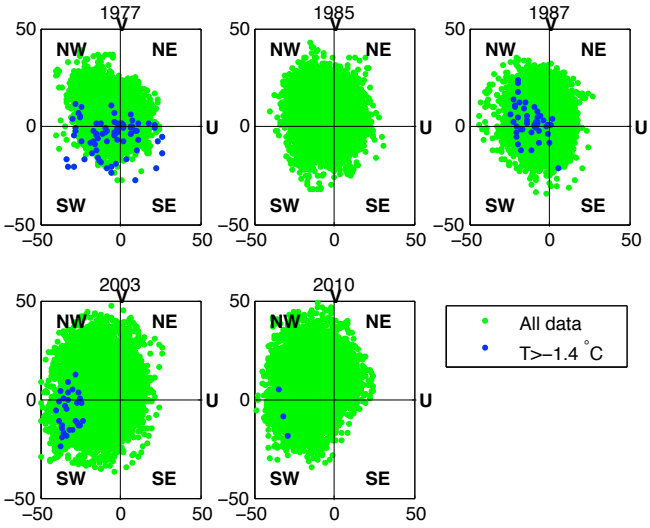

Figure 6.1: Current vectors from the lowest instruments at S2 for 1977, 1985, 1987, 2003 and 2010. The green dots show all data, while the blue dots represent the directions of waters with temperatures higher than −1.4°C.

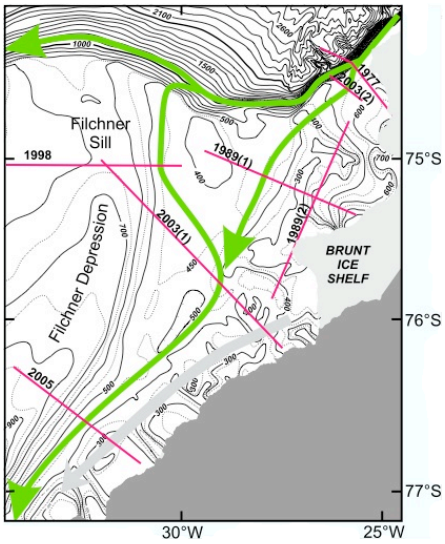

Figure 6.2: Figure from Nicholls *et al.* (2009) showing currents onto the Filchner continental shelf; flow of MWDW (green arrow) and a coastal current (grey arrow) determined from the indicated hydrographic sections.

6.2 Seasonal variation in ISW

Seasonal signals have been detected in the data from the moorings investigated; south of Filchner Sill (FR1) and at the Filchner Sill (S2).

S2

Seasonal signals have been detected in the temperature data for all levels (see figures 5.5(a) and 5.5(b)). Although the amplitudes are smaller at the lowest instruments, the same signals are found. The highest temperatures are measured during late austral summer/early fall, and the lowest are measured during austral winter/early spring. The warm phase is longer than the cold phase. The seasonal signal for the lowest instruments at S2 are ranging from 0.04 to 0.09°C. Especially the years 1985, 2003, 2009 and 2010 clearly show seasonal oscillations, although the 2003 data are warmer (this will be discussed later in section 6.3). The temperature series at S2 in 1985, 2009 and 2010 have been measured independently with different instruments (a Aanderaa RCM 7 in 1985, a Aandera RCM 9 in 2009 and a Microcat in 2010) and depths (25 m above bottom in 1985 and at the bottom in 2009) raising the confidence that a seasonal signal exists in the ISW plume over the Sill. Temperature at the deepest instrument in 1977 show a "normal" seasonal oscillation pattern until around September, when the temperature continue to drop. The 1987 temperature series seem to follow the seasonal oscillation until around October when the temperatures starts to rise towards -1.9°C. A further discussion of these observations are done in section 6.3.

Figure 5.14 show the normalized salinity and temperature data from 2009. It appears that the salinity data exhibits a similar seasonal cycle as the temperature. The correlation between temperature and salinity has been calculated for the low-passed filtered data. The correlation is found to to be ~ 0.66.

From a first look at the current speed series (figure 5.9) seasonal signals seem to be comparable to those of temperature and salinity, with lowest speeds in late winter/early springs and maximums during summertime (except in 2003). Correlation between the 100 days averaged current speed and temperature data for all years have been found. The correlations are found to range from $\sim 0.48 - 0.85$ for the different years, except in 2003 where there is a negative correlation of ~ -0.53.

FR1

The instrument 20 m above bottom southeast of S2 show a seasonal signal (figure 5.8). The temperature data have been averaged over 30 days, and the seasonal signal is found to be 0.1°C supporting the observations of seasonal signals at S2.

Hypothesis 1

It has previously been implied by Grosfeld *et al.* (2001) and Nicholls *et al.* (2003) that the ISW reaching S2 has obtained its characteristics by mixing with ambient water masses along its path in the Filchner Depression. The conditions for mixing is assumed to change from winter to summer. This gives the first hypothesis:

ISW from underneath the FRIS has no seasonal signal, i.e. its temperature (T_{ISW}) is constant throughout the year. The seasonal signal observed at the Sill therefore need to come from mixing between ISW and ambient water masses in the Filchner Depression.

Grosfeld *et al.* (2001) proposed that the ISW plume reaching the Filchner Sill has increased in size by admixture of both MWDW and HSSW. A distribution of MWDW over the continental shelf shown in Foldvik *et al.* (1985d) , however, shows only MWDW at the outer rim of the Filchner Depression indicating that MWDW is mostly outside ISW's "mixing path". In fact no MWDW is seen at the FR1 mooring south of the Sill (figure 5.8), giving more confidence that the mixing component is not MWDW. It is then assumed that the mixing component of the ISW at S2 is HSSW (T= -1.9°C). The characteristics of HSSW is assumed to be constant throughout the year, which is reasonable since its temperature is defined as the surface freezing point. The temperature of the ISW at S2 (T_{FS}) is varying from the summer maximum ($T_{FS_{summer}}$) to winter minimum ($T_{FS_{winter}}$) found in the FFT seasonal curve for the lowest instruments at S2 ($T_{FS_{summer}} = -1.97$°C and $T_{FS_{winter}} = -2.03$°C, respectively). How much in-mixed HSSW needs to be added to the ISW with winter temperatures to increase the temperature by 0.06°C reaching summer temperatures of the ISW?

In order to test hypothesis 1, the amount of increased mixing needed from winter to summer can be calculated with a set of equations (similar to the equations used in Foldvik *et al.* (2004))

$$T_{HSSW} * X_{HSSW} + T_{FS_{winter}} * X_{FS_{winter}} = T_{FS_{summer}} \tag{6.1}$$

$$X_{HSSW} + X_{FS_{winter}} = 1 \tag{6.2}$$

where $T_{HSSW}, T_{FS_{winter}}$ and $T_{FS_{summer}}$ are the temperatures of the in-mixed HSSW, the ISW observed at the Filchner Sill during winter and the ISW at the Filchner Sill during summer, respetively. X_{HSSW} and $X_{FS_{winter}}$ are the fraction of admixed HSSW and fraction of ISW at the Filchner Sill in wintertime, respectively.

Combining equations 6.1 and 6.2 gives:

$$X_{HSSW} = \frac{T_{FS_{(summer)}} - T_{FS_{winter}}}{T_{HSSW} - T_{FS_{winter}}} \approx 0.46 = 46\% \tag{6.3}$$

The summer plume of ISW at S2 therefore consists of 46% HSSW and 54% "winter"-ISW, which is an almost volume doubling. This is too high compared with the velocities within the Filchner Depression. To put this value into context, a comparison has been done with the mixing occurring in the Filchner Overflow. The WSBW (referenced to $-0.8°$C) produced by a mixture of ISW and MWDW is found to contain 63% in-mixed MWDW (Foldvik *et al.* , 2004). This implies that the seasonal signal cannot fully be accounted for by seasonal difference in mixing, leading to the second hypothesis.

Hypothesis 2

ISW flowing out of the Filchner Ice Shelf cavity has a seasonal signal.

Site 5

For this analysis the temperature data from Site 5 placed underneath the FRIS southwest of Berkner Island are used (see figure 2.2). Figure 6.3 shows the temperature data from Site 5 as used in the article by Nicholls & Østerhus (2004). As mentioned by Nicholls & Østerhus (2004) this data set contains both seasonal signals and interannual variability. The seasonal signal underneath the Filchner-Ronne Ice Shelf has in addition been discussed by Nicholls (1996).

The observations made by Nicholls & Østerhus (2004) can be summarized as follows; first a large pulse of HSSW is detected. This pulse is formed from the

anomalously large polynya outside the Ronne Ice Front during the Austral summer 1997/98. The same pulse returns to Site 5, after recirculated in the ice shelf cavity, as anomalously cold waters around mid-2000/2001. In 2002 the water characteristics are assumed be returned back to "normal". The data from 2002 are therefore used in this investigation.

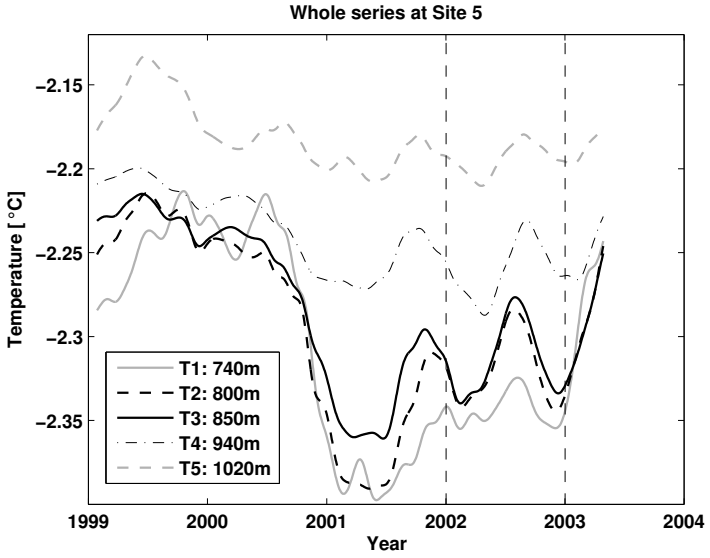

Figure 6.3: The 100 days filtered temperature data from the Site 5 mooring. The instruments are shown in an order starting with the topmost instrument (T1) to the lowest instrument (T5) with approximate depths below sea level.

The seasonal signal underneath the ice shelf is a result from external forcing outside the ice front (Nicholls, 1996). Using 100 days filtered data from 2002, the seasonal signals for all the instruments have been found to range from $0.03 - 0.06$°C with peak temperatures around August and minimum temperatures around February. Instruments T2 and T3 (see figure 6.3) with seasonal range of 0.06°C are, according to Nicholls & Østerhus (2004), placed in the ISW plume originating from Berkner Bank and are therefore chosen for this study because this is the pathway assumed to be light enough to escape the cavity reaching the Filchner Sill. The mean seasonal signal of these two instruments in 2002 are shown in figure 6.4.

The seasonal signal at the deepest instruments at S2 is ranging from 0.04 to 0.09°C, indicating that at least some of the signal may be explained by the variations within the ISW plume itself. If this is true, there is a time lag of about $\sim$8 months from Site 5 to S2 (peak at Site 5 in August reaches S2 in April the

next year, see figure 6.4). Assuming that the distance from Site 5 to S2 is $\sim$ 1000 km, gives an average velocity of 5 cm/s between the sites. This is reasonable. At least some of the seasonal signal found at S2 should therefore originate from outside the Ronne Ice Front.

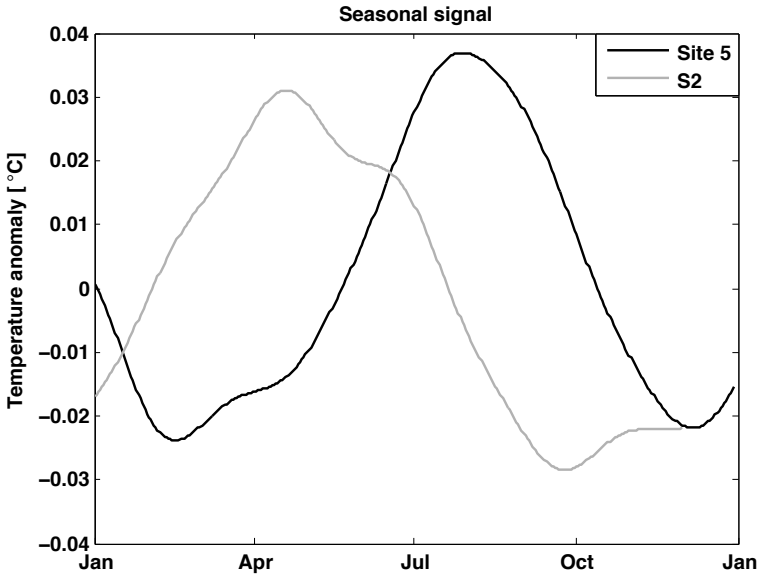

Figure 6.4: The figure show the time lag between the seasonal signals at Site 5 and S2. The black curve is the 100 hours low-pass filtered temperature anomaly in 2002 at Site 5 calculated from the mean of instrument T2 and T3. The grey curve is fast fourier transformed seasonal signal for the bottom layers at S2.

6.2.1 Summary

The first article (Foldvik *et al.* , 1985b) covering the time series from S2 did not find any seasonal signal. This was because the only available measurements were from 1977. No later articles have discussed the specific ISW variations at S2. But seasonal signals have been discussed in the HSSW at the Ronne Ice Front by Foldvik *et al.* (2001) and in the ice shelf cavity by Nicholls & Østerhus (2004) and Nicholls (1996). A connection of the variability from the Ronne Ice Front and the ice shelf cavity was found. From the investigation done there, there is confidence to suggest that some of the seasonal signal in the ISW at S2 originates from outside the Ronne Ice Front. The mixing needed in the Filchner Depression to account for the seasonal signal is too high to be the only explanation.

6.3 Interannual variations at S2

There are detected year-to-year variations (even in this scattered data set), which will be discussed here.

6.3.1 1977

The temperature series from 1977 is colder than the other years with no seasonal signal. Around September 1977 a "negative trend" is seen in the temperature (and current speed) series closest to the bottom. The negative trend is measured between late September and until the instrument stopped recording in March 1978. This is the Austral spring and summer season, when the temperatures should start to rise again (see figure 5.2(a)).

Calibration

The CTD section taken when the moored instruments were recovered does not show any clear difference compared with the other years (figure 5.11(b)). Calibration with CTD for the end of the series is not comparable since the CTD section was taken in February 1979 and the S2 mooring stopped recording in March 1978 ($\sim$one year earlier). Unfortunately the upper instrument stopped recording around the same time as the negative trend started (figure 5.2(a)). The current data at 25 m above bottom in 1977 show a similar signal with decreasing velocities (see figure 5.9). A high linear correlation is found to be ~ 0.85. This means that two independently sensors measured similar signal, giving confidence that the trend is unlikely to come from a sensor drift. In other words, the ISW plume gets colder and slower throughout the year in 1977.

Buoyancy loss

When this mooring was recovered, it was discovered that its buoyancy was poor (Nygaard, 1994), expecting the instrument to have sunk down to deeper levels than the intended depth of 25 m.a.b. Since the water should be colder closer to the bottom due to the density stratification, and the speed should be lower due to the bottom friction, it was assumed that the bad buoyancy was the reason for the discrepancy of the data at the lowest instrument at the S2 in 1977. But after the recovery of the S2 2009 mooring placed at the bottom, showing "normal" temperature variations, the buoyancy argument has lost its significance.

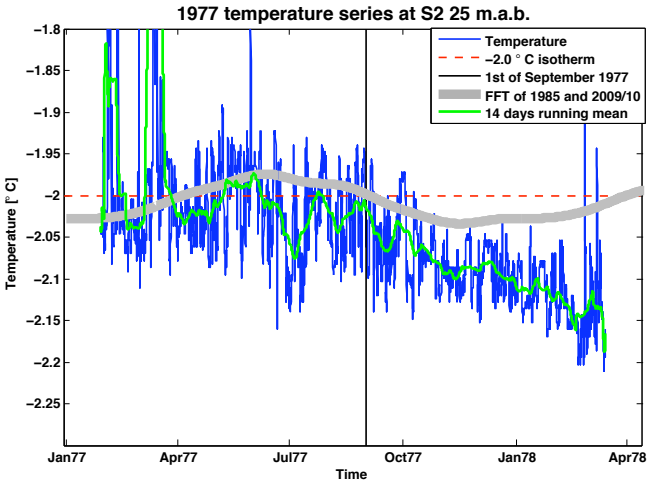

Figure 6.5: 30 hours butterworth filtered temperature data from 25 meters above bottom at S2 in 1977 (blue line), the 14 days running mean (green line), the −2.00°C isotherm (red dash-dotted line) and the interpolated seasonal curve using fast fourier transformation (thick grey line). 1st. of September is in addition marked (black vertical line).

Theoretical considerations

With these considerations taken into account, the next step will be to investigate physical explanations for the observed discrepancy.

In general: To get ISW temperatures down to −2.2°C (figure 6.5), the water mass need to have high salinity, or originate from the deeper parts underneath the Filchner-Ronne Ice Shelf (see equation 3.1).

Why has this happened, and how is this water mass able to escape over the Filchner Sill passing S2? A few possibilities are listed to shed light over the problem:

1. From the "second seasonality-hypothesis" it could be due to a year of anomalous forcing at the Ronne Ice Front some 5-10 years underneath the Filchner-Ronne Ice Shelf (Nicholls & Østerhus, 2004; Gammelsrød *et al.* , 1994) prior to 1977 for the deepest ISW (from Ronne Depression) or $\sim$ 2 years for the warmest ISW (from Berkner Bank (Nicholls & Østerhus, 2004)).

2. If the seasonality come from mixing with ambient water masses, and not from the conditions in front of Ronne Ice Shelf, the mixing regime during Summer of 77/78 should be different compared to the other years with available data.

CTD sections taken over the Filchner Sill compared with the ones further south (figure 5.11) show that the ISW plume is coldest in the south. As long as the ISW plume is able to flow northwards towards the Filchner Sill with reduced mixing during the summer, this could explain the lower temperatures.

3. The stratification in the Filchner Depression could be different compared with the other years, making "colder than usual" waters able to cross the Filchner Sill. The CTD cross-section south of Filchner Sill in 1977 (figure 5.11(c)) show that the deeper layers of the Depression are filled with HSSW. The stratification is discussed by Foldvik *et al.* (1985a), which explained that HSSW drain from Berkner Bank into the bottom of Filchner Depression. The ISW plume from the ice shelf cavity flows above the HSSW. If 1977 was a year of anomalous large production of HSSW on Berkner Bank, a thicker layer of this denser water mass could force the colder ISW core to levels where it is able to cross the Filchner Sill.

4. If the contribution of ISW originating from Berkner Bank decreased (no HSSW flows under the ice shelf from Berkner Bank), the only water available flowing out into Filchner Depression from the cavity would be the recirculated ISW originating from Ronne Depression, that have reached deeper levels before flowing out of the cavity (see figure 2.2).

5. During the time interval in question, a special feature reoccurred in the Weddell Sea. A large polynya named the Weddell Polynya formed over Maud Rise in wintertime from 1973 to 1977, each year appearing more westward from 40°E towards 20°W (Martinson *et al.* , 1981), see figure 6.6. This huge polynya had a cooling effect of the WDW in the Weddell Sea (Gordon, 1982; Foldvik *et al.* , 1985a). Since the WDW is a component of MWDW, it is an important water mass in the formation of HSSW, and hence in the formation of ISW. A change in WDW could therefore possible change the oceanographic conditions leading to the formation of ISW. This may have an impact on the production of HSSW. Gammelsrød *et al.* (1994) found that the WDW increased by 0.7°C since 1977, giving higher confidence that the year 1977 had extraordinary WDW.

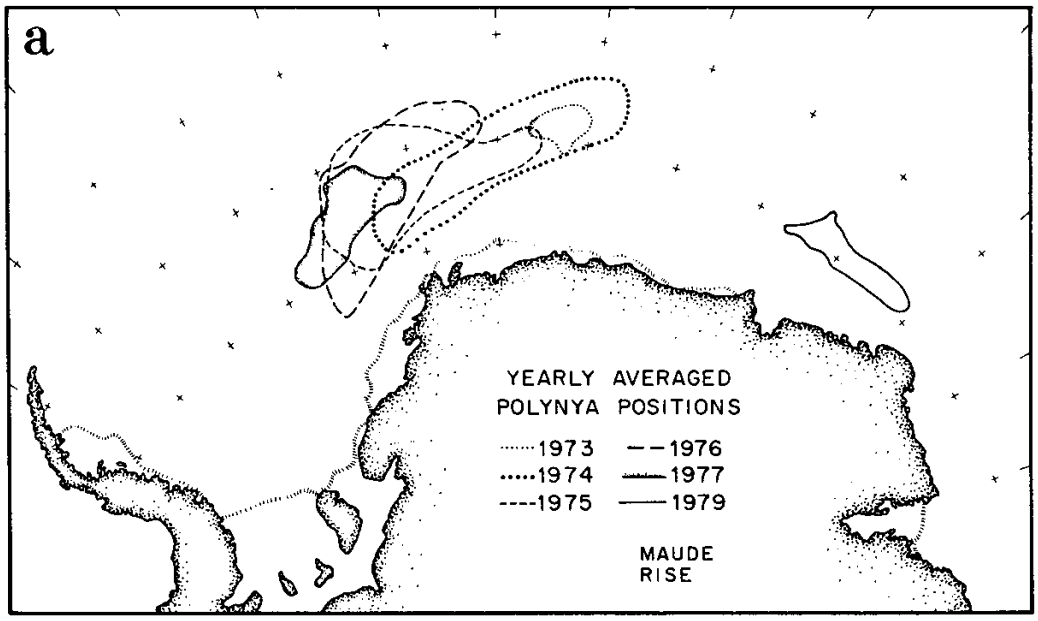

Figure 6.6: The position of the Weddell Polynya during the time period from 1973-1979. The figure is taken from Martinson *et al.* (1981).

Summary

The physical possibilities listed (change in forcing at the Ronne Ice Front, mixing, stratification, detachment from the ice shelf and/or change in HSSW formation) may all (to some degree) be explained by a change in atmospheric forcing or a change in sea ice conditions. The oceanic view is possible quite complex, and a more thorough investigation is therefore needed before any conclusions might be drawn.

6.3.2 1985

Looking at figure 5.4, the exception of warm intrusion at the deepest instrument at S2 is the year 1985, where there is no evidence of MWDW reaching the S2 position. Figure 2.4 show that MWDW is located in the eastern part of the Filchner Sill, indicating that the intrusion is intermittent and during this particular year it did not reach as far west at the Sill as the S2 (the S2 position is comparable to CTD station # 11 in figure 2.4). Since the summer intrusion is thought to be a result from atmospheric forcing, there might have been differences in these forcings this particular year, changing the MWDW circulation.

6.3.3 1987

The S2 1987 temperature series 25 m above bottom seem to follow the seasonal variation until around October (spring towards summer) when the temperatures starts to rise towards $-1.9°C$. At the same time as the temperatures increases at the bottom towards HSSW characteristics, the upper instruments starts measuring lower temperatures towards ISW characteristics, i.e. HSSW is now below ISW at the Sill (see figure 5.2(c)). Meanwhile the current direction changes from a northwestward direction to a more northward direction (see figure 6.9). These changes coincides with the grounding of three huge icebergs on the Berkner shelf.

The iceberg break-off event

In August 1986 three huge icebergs, named A22, A23 and A24, broke off the Filchner Ice Shelf (Grosfeld *et al.* , 2001) and drifted northwestward (figure 6.7(a)). With an average thickness of ~ 400 m, the icebergs grounded on Berkner Bank in late 1987 or early 1988 (Nøst & Østerhus, 1998). Crevasses in the Filchner Ice Shelf had been monitored since the 50s (Campbell, 1998). The calving event was unique since the Filchner Ice Shelf may only experience such a major ice loss event (40 years worth of advancing ice) once or twice each century (Campbell, 1998). In 1990, iceberg A24 broke free from Berkner Bank and moved northward (Campbell, 1998). The remnants of the other two remain on Berkner Bank to the current date (see figure 6.7(b) for an illustration).

The break-off of the icebergs along the Fichner Ice Front caused a change in the ice draft, which may have caused a change in the depth where ISW flows out from underneath the Filchner Ice Shelf (change in depth of neutral buoyancy, i.e. detachment depth).

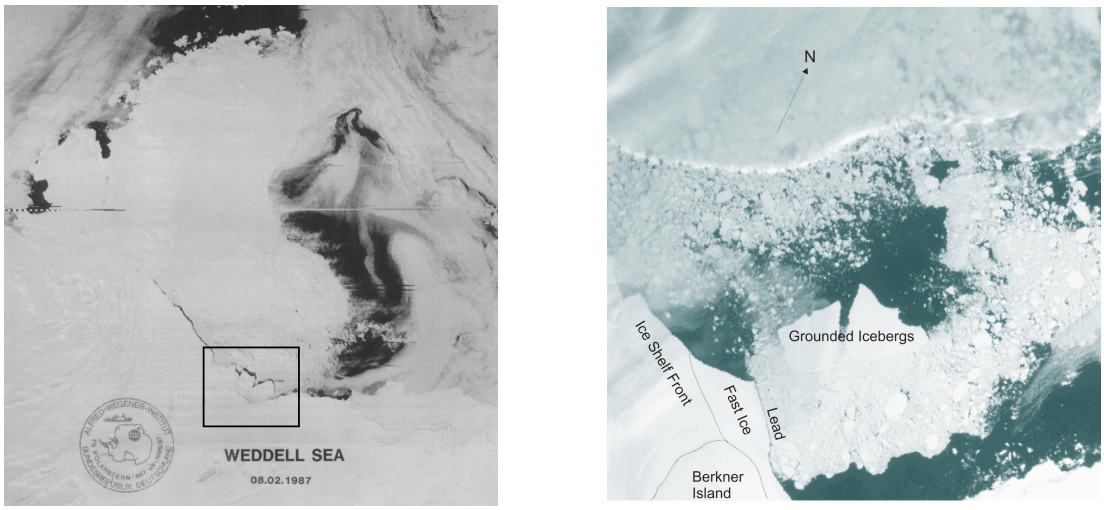

(a) February 1987 (b) February 1993

Figure 6.7: a) Satellite image showing the icebergs in February 1987 (black frame) (courtesy to Svein Østerhus). b) The ice conditions on Berkner Bank in 1993 with grounded icebergs. Satellite picture is taken from Foldvik *et al.* (2001).

Nøst & Østerhus (1998) examined CTD casts taken in the Filchner Depression from 1980 to 1993. They found a cooling of the water at the bottom of the Filchner Depression due to this particular grounding event. The cooling occurred because of a shift from HSSW to ISW at the bottom of the Filchner Depression. HSSW usually drain from Berkner Bank into the bottom layers of the Filchner Depression (Foldvik *et al.* , 1985d). This drainage reduced because of the barrier-effect of the icebergs that started between February and October 1987 (Nøst & Østerhus, 1998), coinciding with the observations in this thesis. Since ISW has a lower density than HSSW (due to less salinity), the ISW able to flow out of the ice shelf cavity may have a deeper detachment level. Colder ISW will hence be able to escape from the cavity, decreasing the temperature of the ISW in the Filchner Depression (Nøst & Østerhus, 1998).

In addition, the grounded icebergs at Berkner Bank created artificial islands disrupting the sea ice flow in the Weddell Gyre (Markus, 1996). This lead to a change in the sea ice conditions, getting a pile up of ice along the east side of the icebergs, and less sea ice along the west side (Nøst & Østerhus, 1998). A change in sea ice conditions might lead to a change in the sea ice formation, and hence a change in HSSW formation on Berkner Bank and north of the Filchner Depression (Markus, 1996).

Grosfeld *et al.* (2001) examined the grounding event using a numerical model. The main conclusion was that the flow of HSSW from the Berkner Bank into the Filchner Depression was reduced. The circulation in the ice shelf cavity became less active because of this reduction. The HSSW on Berkner Bank were modeled to flow around the icebergs entering the Filchner Depression system north of the icebergs. Figure 6.8 shows the modeled path of the HSSW formed on the western side of the icebergs. The HSSW is flowing northeastward around the icebergs getting deflected by Coriolis to the north just before the Filchner Sill (Grosfeld *et al.* , 2001).

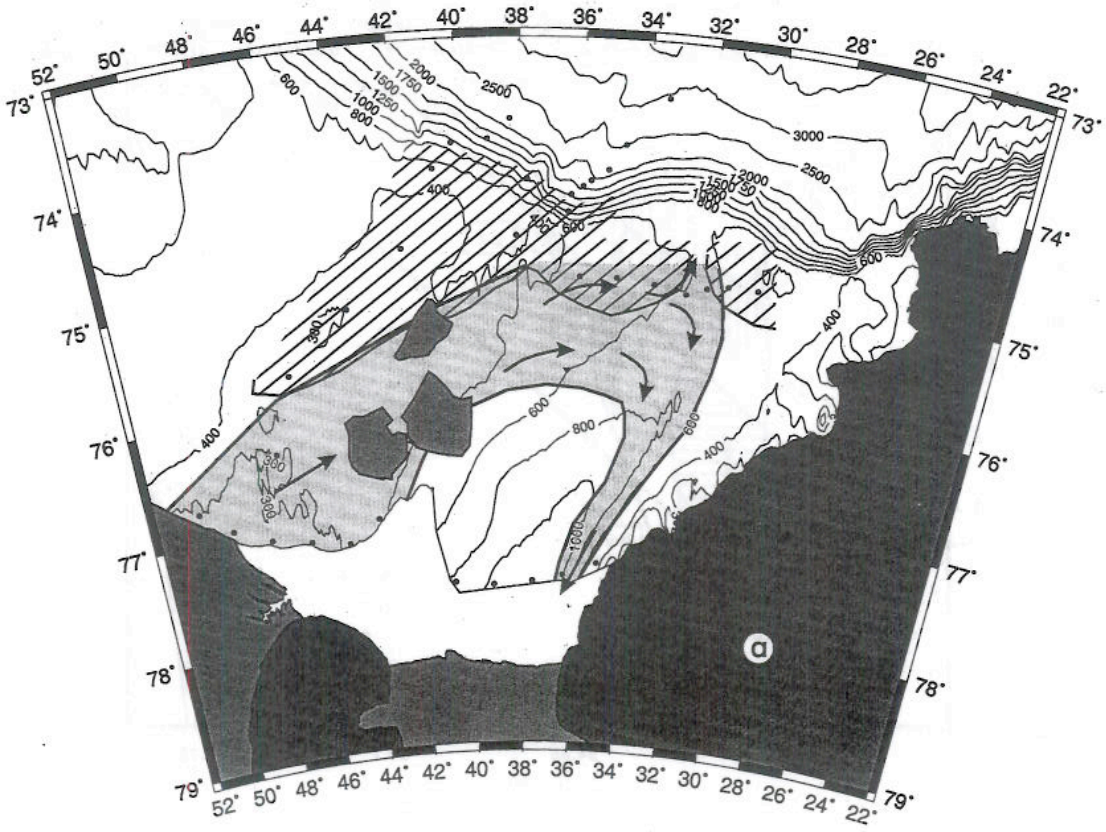

Figure 6.8: The modeled horizontal HSSW flow (shaded and schematically shown with arrows) after the grounding event in 1987. The figure is taken from Grosfeld *et al.* (2001).

It is clear from figure 6.9 that the current at the S2 position changed to a more northerly path after October 1987, which is the time when the icebergs arrived at Berkner Bank (Grosfeld *et al.* , 2001). This shift in direction is not seen other

years (see figure 5.10). It is around the same time the temperatures shifts from ISW to HSSW characteristics at S2 25 m above bottom (see figure 6.10). The instrument at 100 m above bottom shifts towards ISW characteristics (see figure 5.2). Due to the higher density of HSSW than ISW this is expected to happen if HSSW enters the Filchner Sill.

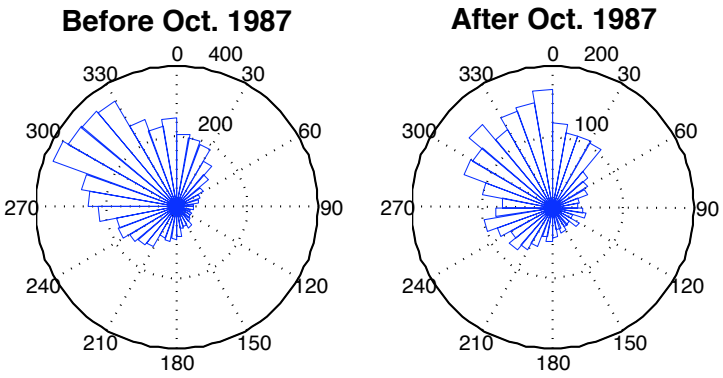

Figure 6.9: Rose diagram of current directions at the deepest instrument at S2 in 1987 before and after October.

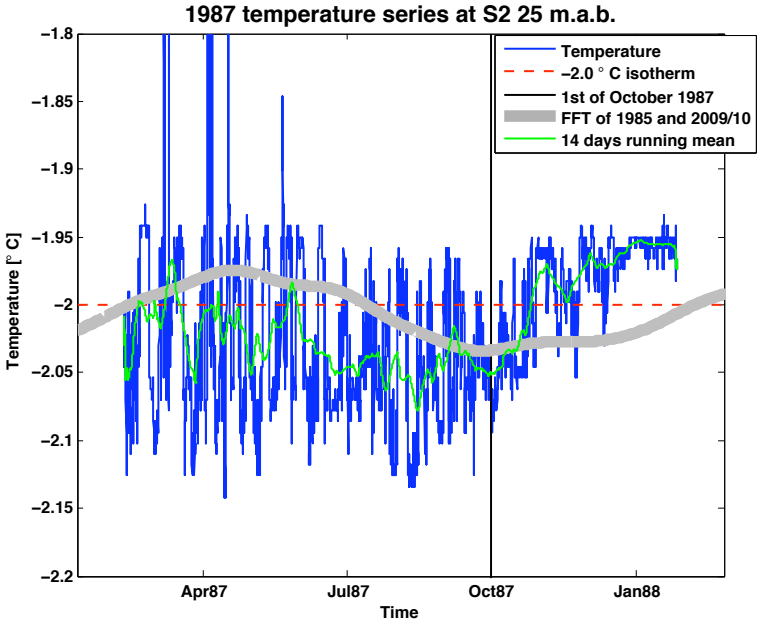

Figure 6.10: 30 hours butterworth filtered temperature data from 25 meters above bottom at S2 in 1987 (blue line), the 14 days running mean (green line), the $-2.00°C$ isotherm (red dash-dotted line) and the interpolated seasonal curve using fast fourier transformation (thick grey line). 1st. of October is in addition marked (black vertical line).

Summary

The observed change in directions and temperatures on the Filchner Sill from pre- to post-calving times fits quite well with the modeled results from Grosfeld *et al.* (2001). This indicates that the change in circulation and formation of HSSW on Berkner Bank most likely are the dominating effect causing the observed temperature increase at Filchner Sill in late 1987.

6.3.4 2003

Figures 5.2(d), 5.4, 5.5(b) and 5.12 show that there are relatively high temperatures at S2 in 2003 compared with the rest of the time series available (25 m.a.b.). The temperatures series have little variation and are closer to HSSW than ISW. Calibrations with CTD-casts have been done, and the data seem to correspond well with the CTD taken when the mooring was deployed.

The $\theta - S$ diagram (figure 5.13) clearly confirm (like the other figures: 5.2(d), 5.4 and 5.5(b)) that in this respective year the ISW plume over the Filchner Sill has little variation in temperature compared to the other years investigated. Looking at fig. 5.10 the S2 ISW plume have higher current speeds and a more westerly direction compared to the current data available from previous years. A negative correlation of -0.53 is found between the current speed and the temperature.

To summarize, the ISW plume in 2003 has higher speeds and less variance in the temperature compared with previous years. This is the only year with available data from the bottom layers at the Filchner Sill where there is found a negative correlation between the current speed and temperature data. Why did this discrepancy happen in 2003?

Looking at figure 4.1, the S2 2003, as well as the S2 mooring from 2009 and 2010, are located further east in an area of steeper topography than S2 1977, S2 1985 and S2 1987. The current data in 2010 show the same behavior as in 2003, indicating that the higher current speeds may be a result of topographic steering. The temperature series from 2009 and 2010, however, show similar temperatures to the pre-2003 state, indicating that the different location is not the reason for the high temperatures in 2003.

What caused the high temperatures?

In 1990, one of the grounded icebergs left Berkner Bank and the system began to switch back to its original hydrographical state (Grosfeld *et al.* , 2001). The effect of the grounded icebergs should therefore be reduced by the year 2003. If the higher temperatures observed in 2003 are the result of the still-grounded icebergs, the instrument 100 m above bottom should be filled with ISW, as in the end of the 1987 series. Comparing figure 5.2(c) and 5.2(d)) confirm that this is not the case, and the temperature discrepancy is not due to the grounded icebergs at Berkner Bank.

The observed interannual variability at Site 5 (southwest of Berkner Island) was explained by the variability of the processes north of the Ronne Ice Front (Nicholls & Østerhus, 2004). Winds and tidal motions maintain shore leads and polynyas and the winter freezing deposits pulses of HSSW into the water column. These salt pulses eventually flow into the ice shelf cavity transforming into ISW by the interactions with the glacial ice. The strength of the pulses depends on the size of the open water area. An anomalously large polynya occurred outside the Ronne Ice Shelf Front during the Austral summer of 1997/1998 due to strong southerly/southwestly winds. The response was observed at Site 5 as a large pulse of HSSW in 1999. (Another major event during 1998 was the breakup of the eastern Ronne Ice Front, but the polynya event dominate over the icebergs in affecting the HSSW production (Nicholls & Østerhus, 2004).) The large pulse of HSSW, with expected high speed, was observed as an extraordinary cold pulse of recirculated ISW in 2001 because it was too dense to escape the Depression (Nicholls & Østerhus, 2004).

Following up the hypothesis that the seasonal variations at S2 have been propagating under the ice shelf, the anomalously large pulse of very cold ISW should again have reached the Filchner Depression. Still too dense to escape the Filchner cavity, it may make the warmer ISW core from the Berkner Bank the only contribution flowing over the Filchner Sill. The negative correlation between current speed and temperature, increases the suspicion that this is a year with extraordinary ISW characteristics.

Summary

From the discussion about the seasonal signal, the relative uniform temperatures in 2003 should be an effect of an anomalous forcing in front of the Ronne Ice Shelf. A possible explanation is that the anomalously cold ISW plume from the 1997/98 polynya discussed by Nicholls & Østerhus (2004) made the warmer ISW from Berkner Bank the only contribution able to escape the ice shelf cavity.

6.4 Long-term trends

Having one of the longest oceanographic data sets in Antarctica makes it tempting to investigate long-term trends, although it is admittedly a limited data set, with six year-long temperature series spread over 30 years.

Looking at figure 5.4 the temperature of the ISW has only varied between $-2.20°C$ and $\sim -1.90°C$ showing no long-term trend. If data were only available up to 2003, a positive trend could have been suggested, but the later time series at S2 (in 2009 and 2010) show temperatures similar to pre-2003 state.

Since the ISW gets its low temperatures from the interactions underneath the Filchner-Ronne Ice Shelf, the temperature of pure ISW should only vary around the freezing point of seawater for different salinities and different depths. By knowing that the maximum depth underneath the ice shelf is $\sim$ 1500 m one should expect a maximum theoretical temperature range of $\sim 1.15°C$ ($[-1.90$ to $-3.05°C]$) for the salinity range of the parent HSSW found over the continental shelf ($34.6 - 34.8$). The Filchner Sill with its depth of $\sim$ 600 m has a local freezing point of $\sim -2.35°C$ for the same salinity range, indicating that this is the lowest temperature one can expect at the Sill without the water being in-situ supercooled (if the ISW is in-situ supercooled, formation of frazil ice would most likely occur). The temperature range expected in the ISW at the S2 position is therefore assumed to be $\sim \Delta T = 0.45°C$. As long as the Filchner-Ronne Ice Shelf persists with cold core temperatures and its ice shelf cavity, and the water masses flowing into the cavity have sub-zero temperatures, the ISW formed is expected to vary within this temperature range. There are variations in the ISW characteristics, which probably are dependent on the forcing outside the ice shelf, and long-term trends cannot be ruled out in the future if the oceanic conditions and/or the atmospheric forcing outside the ice shelf experiences any long-term trends.

6.5 Dissolved Oxygen

The dissolved oxygen data are not used in the main discussion, but included here since this is the first year-long time series of O_2 in the southern Weddell Sea. Two independent year-long dissolved oxygen series were recovered in 2009 for the first time at the bottom of Filchner Sill. Figure 5.15 show that the dissolved oxygen levels are not higher than the saturation level for given salinity and temperature. A positive trend (figure 5.15) is seen in both data sets. According to the manufacturer (Aanderaa, pers. com.) a sensor drift should give a negative trend, giving more confidence in the data. The de-trended data set are shown in figure 5.16 together with the salinity data. Negative correlations are found to be ~ 0.7 between oxygen and temperature, and ~ 0.8 between oxygen and salinity in the filtered data sets. This high negative correlation is illustrated in figure 5.16. Negative correlations are expected since the solubility of gases generally increases with decreasing temperature and salinity (Brown & Bearman, 1999). So the oxygen seem to correlate well with the observed salinity and temperature oscillation. The attribution from the ice shelf interactions (melting) will decrease the amount of oxygen in the waters because of the addition of glacial meltwater. A thinkable attribution to *increased* oxygen have to come from the atmosphere. But there is no obvious reason for why there should exist a positive trend in the oxygen data. Oxygen is a tracer characteristic that should be further investigated in order to increase the understanding of the formation and behavior of ISW. Hopefully there will be obtained more year-long oxygen data sets in the future.

7

Conclusion

Variations are found in the ISW characteristics at Filchner Sill (the S2 position), from seasonal to interannual variations. The seasonal signal in the ISW has previously been explained as being the result of the admixture of ambient water masses along its path from the Filchner Ice Shelf Front to the Filchner Sill (Grosfeld *et al.* , 2001; Nicholls *et al.* , 2003). From this analysis, however, the ISW flowing out of the ice shelf cavity contains a seasonal signal itself, indicating that the forcing in front of the Ronne Ice Shelf generates the seasonal signal in the ISW plume flowing over the Filchner Sill. Interannual variations in the ISW characteristics are found to be results from changes in the sea ice cover and the occurrence of grounded icebergs. No long-term trend in the ISW temperatures is found, which are expected since the physical properties are controlled by the Filchner-Ronne Ice Shelf system.

8

Future work

Previous calculations of WSDW and WSBW from ISW have been done by assuming constant characteristics of the ISW overflow (e.g. (Weppernig *et al.* , 1996)). By understanding the variability of the ISW characteristics, more precise estimates of the bottom water formation may be calculated. Parameterizations of the behavior of the ISW plume may give an improved representation of the Filchner Overflow in climate models. It may even be possible to correlate between the variability of the AABW and ISW. As the variability of the ISW characteristics may be described by the atmospheric forcing and sea ice anomalies in front of the Ronne Ice Shelf, remote sensing might be used as a prediction system for estimating the ISW overflow. McKee *et al.* (2011) investigated temporal variations in the bottom water from the Weddell Sea relative to larger scale climatic fluctuations, as the El Niño/Southern Oscillation (ENSO), Southern Annular Mode (SAM) and Antarctic Dipole (ADP). The data used were from a mooring site just south of the Orkney Islands and contained 8 years of data. Combining the findings by McKee *et al.* (2011) with this work and additional observations from the Weddell Sea, may be a natural next step.

Appendix A

Supplement to Instruments and Methods

The analysis of the data have been done using Matlab R2009b for Mac OS X. The same is the case for all the figures. The time series are low-pass filtered using a 7th. order Butterworth design with cutoffs specified in the text. In some cases running means have been used The main focus have been on temperature. Calibration with the closest CTD casts available are done for the temperature senosors on the current meter instruments, see appendix B.

A.1 Mooring Instruments

Table A.1: Overview of the long-term S2 moorings (as well as FR1). Columns show deployment year, latitude, longitude, bottom depth, deployment vessels and cruise names.

S2 moorings					
Year	**Lat.**	**Lon.**	**B. Depth [m]**	**Vessel**	**Cruise name**
1977	-74 40	-33 56	558	Polarsirkel	NARE 76/77
1985	-74 40	-33 56	545	Andenes	NARE 84/85
1987	-74 40	-34 00	558	Polarstern	ANT 5/4
2003	-74 40	-33 28	597	Ernest Shackleton	NARE 02/03
2009	-74 39	-33 33	602	Ernest Shackleton	BIAC
2010	-74 38	-33 30	612	Ernest Shackleton	NARE 10/11
FR1 mooring					
1995	-75 01	-31 46	610	Polarstern	AWI

Recording Current Meter (RCM)

Calibration is needed to compensate for drift of the sensors. RCM instruments have six channels; reference, temperature, salinity, pressure, speed, and compass direction. In general are the recorded temperatures reliable, but the salinity (conductivity) need substantial calibration. RCM's inductive conductivity sensors are bad compared to the conductive sensors of the CTDs.

Background

The Recording Current Meter 4 instrument (first called the Bergen's current measurer) fabricated by Aanderaa Instruments A/S in the 1960s was the first instrument that were able to record currents for a whole year. Due to the possibility of getting a yearly time series in remote areas this mark the beginning of the modern Norwegian oceanographic Antarctic research. In 1977 the Norwegian Antarctic Research Expedition (NARE) deployed a mooring containing two RCM 4 instruments measuring velocity and temperature at the Filchner Sill.

RCM 4/7/8

The main improvement of the RCM from 4 to 7 is that the storing of data is digitalized, no longer recording on tape. The RCM 7 now also contain an inductive conductivity cell which measures the water's ability to conduct and a pressure sensor. The only improvement from RCM 7 to RCM 8 is a more robust instrument shell that can handle higher pressure.

With this in mind, this time series are quite homogeneous due to the use of similar instruments.

RCM 9 IW

The improvement from RCM 8 to RCM 9 is in the conductivity cell and the way currents are measured. The rotor measuring current in one point is replaced by an acoustic doppler current sensor measuring the current in several vertical layers with four transmitters. (In general you only need three transmitters, but the fourth is a quality check.) The temperature sensor is made of platinum which means that the precision is determined by the electronics. The RCM 9 IW manufactured by Aanderaa Instruments A/S, is a RCM 9 modified to measure temperature, oxygen, conductivity and pressure.

The pressure sensor was set to measure at a depth range of 400-600 m, but the instrument was placed at a depth > 600 m and therefore there is no time series of the pressure and it is assumed to be constant in order to calculate the salinity. There were two temperature sensors on the RCM 9 IW. The accuracy of temperature sensor 4050 is ±0.03°C. The temperature sensor 3621 was set to measure in *wide range* instead of *arctic range* which lead to default-values because the sensor was not able to measure in such low temperatures.

Calibration
All the sensors on the RCM 9 IW needed calibration, and the formula and given coefficients are given in appendix B.

RDCP 602

The RDCP 600 is the newest of RCM instruments from Aanderaa Instruments A/S. The instrument now include a precise oxygen Optode and improved electronics in form of computer setups directly on the instrument so that the scientist itself can go in and specify the measuring area. The RDCP 602 (Recording Doppler Current Profiler) measure vertical current profiles by using acoustic Doppler principles. The instrument also consist of a compass tilt sensor (3777), temperature sensor (3621), conductivity sensor (4019B) and a oxygen optode (3830).

The number 600 means that the acoustic sent out is of 600 kHz measuring a 50-60 m vertical current profile.

The temperature sensor 3621 was chosen to measure in *wide range* instead of *arctic range* which lead to default-values because the sensor was not able to measure in such low temperatures that exist at the bottom under the Sill.

Calibration was set in advance for all sensors.

Seabird Electronics 37SM- SBE 37SM

The 2010 mooring also contained SBE-37 Microcats with initial temeprature accuracy of 0.002°C. This makes it possible to calibrate between independent instruments calibrated at its respective factories.

S2 2009 - Remote acoustic data recovering

The S2 mooring deployed in 2009 has a newly developed acoustic remote system transmitting data to ship or buoy without the need of recovering the whole mooring. The instruments used are a modified RCM 9 (IW) and a RDCP 602 and the instrument frame is bottom installed. The data were downloaded to a ship-based computer with the Develogic software *HAM.Node* using an Acoustic system from Develogic. This is in contrast with the traditionally moorings which have an anchor weight at the bottom, the instruments attached on a kevlar rope topped with floating elements, and the only way to get the data is to release the mooring from its anchor and download the data directly from the instruments themselves.

A.2 Conductivity Temperature Depth Profiler

An overview of the different Conductivity Temperature Depth casts used from the southern Weddell Sea are given in table A.2.

Table A.2: Overview of the CTD instruments used in the southwestern Weddell Sea. N.B. stands for Neil Brown, FSI stands for Falmouth Scientific Inc, and SBE stands for SeaBird Electronics.

CTD											
Year 19-	77	79	80	85	87	90	92	95	98	2003	2010
Type	N.B.	N.B.	N.B.	N.B.	N.B.	N.B.	SBE	FSI	SBE	SBE	SBE
Accuracy	±0.005°C	”	”	”	”	”	±0.003°C	N.B.2	”	”	”

Appendix B

Calibration

ISW is defined as a water mass with temperatures below surface freezing point of -1.9°C. Since ISW passes the S2 position it is therefore expected that the temperatures measured here should have a range around this temperature. From figure B.1 the exception is S2 1977, which has its "base" at $-2.0°C$, giving a difference of 0.1°C below the others. This is the same temperature difference found between S2 1977 and the CTD cast taken when the mooring was deployed, see figure B.2(a).

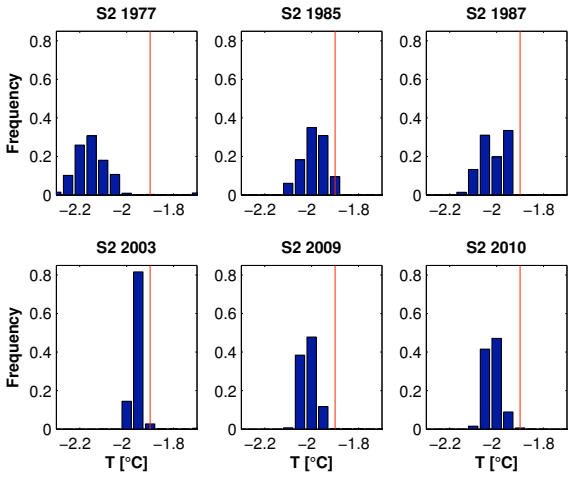

Figure B.1: Temperature frequencies for the deepest S2 current meters. The red line is the $-1.9°C$ isotherm. The temperature interval is $0.05°C$.

Calibration coefficients

The data have been calibrated to physical values using equation B.1, where X are the recorded values by the instruments, Y is the resulting physical data and A, B, C and D are calibration coefficients. The RDCP instrument on S2 2009 was calibrated at Aanderaa Data Instruments A/S. The S2 1987 temperature series at 25 m above bottom (mab) have previously been calibrated using wrong range (wide instead of arctic range (Foldvik *et al.* , 2004)). The old temperature series are shown in yellow in figure B.3. The newly calibrated data are shown in red. Since Seabird Electronics CTDs are more accurate that RCMs all the current meter data will be checked with respect to CTDs in the next section.

$$Y = A + B * X + C * X^2 + D * X^3 \tag{B.1}$$

Conductivity Temperature Depth (CTD)

Calibration of mooring data are done by comparing the different CTD stations occupied when deploying respective moorings. Figure B.2(a), B.2(b), B.2(c), B.2(d) and B.2(e) are showing the daily mean temperature of S2 versus the CTD cast taken the same day for the years 1977, 1985, 1987, 2003 and 2009 respectively. Table B.1 show the temperature difference between moorings and CTD casts. The S2 temperature data from 2010 are in addition compared and checked with a SBE-37 (Microcat) one meter apart at the same mooring line (see figure C.4). The CTD cast sin 1987, 2003 and 2009 did not reach the depth level of the deepest instruments at S2, so the CTD mean is calculated for the lowest points in the profile. Three CTD casts have been used for calibration at S2 2003.

The RCM instrument at 25 m above bottom at S2 in 1977 needed some correction. The time series from 1977 have been calibrated with CTD-measurements taken at the same time and at the same level 1.56 kilometers away from the mooring site. The temperature difference of $0.1°C$ (found in both figures) is subtracted from the whole bottom temperature series of S2 1977. The rest of the instruments seem to compare well within their accuracy with the CTD casts.

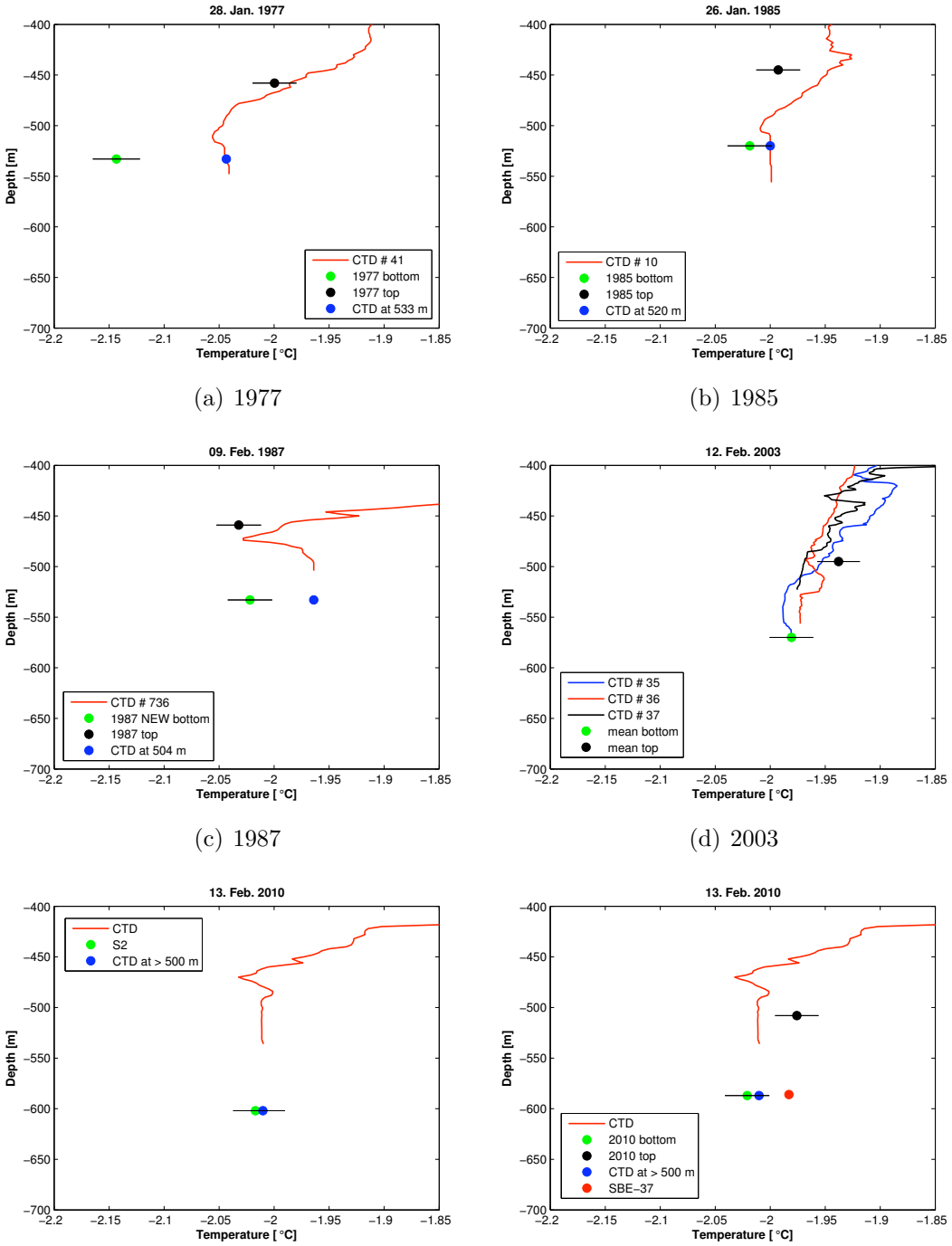

(a) 1977 (b) 1985

(c) 1987 (d) 2003

(e) 2009 (f) 2010

Figure B.2: The red line is the CTD cast taken (date shown at the top of each figure). The green and black dots are the daily mean temperature of the S2 mooring for the top and bottom instrument, respectively. The blue dot is the mean temperature of the CTD profile. Note that the same CTD profile is used for both S2 2009 and S2 2010.

Table B.1: CTD vs current meter instruments. $\triangle T = T_{S2} - T_{CTD}$. *These values are at a different level as the RCM instrument.

Year	CTD #	Distance [km]	Date	Depth [m]	T_{S2}	T_{CTD}	$\triangle T[°C]$	S2 std
1977	41	1.56	28.01	533	-2.1434	-2.0435	-0.0999	0.0031
				458	-1.9997	-1.9860	-0.0137	0.0089
1985	10	0.39	26.01	520	-2.0187	-2.0000	-0.0187	0.0144
				445	-1.9928	-1.9465	-0.0463	0.0121
1987	736	15.06	09.02	533	-1.9721	-1.9640*	-0.0580	0.0196
				459	-2.0322	-1.9915	-0.0407	0.0417
2003	35	15.72	12.02	570	-1.9807	-1.9811*	0.0004	0.0071
				495	-1.9379	-1.9528	0.0149	0.0110
	36	0.88	12.02	570	-1.9807	-1.9644*	-0.0164	0.0071
				495	-1.9379	-1.9664	0.0284	0.0110
	37	13.22	12.02	570	-1.9807	-1.9726*	-0.0082	0.0071
				495	-1.9379	-1.9688	0.0309	0.0110
2009	3	24.47	13.02	602	-2.0170	-2.0102	-0.0068	0.0104
2010	3	22.60	13.02	587	-2.0210	-2.0102*	-0.0108	0.0120
				508	-1.9758	-2.0101	0.0343	0.0094

B.0.1 The calibrated data set

The bottom temperature time series with new S2 1987 calibration and with corrected S2 1977 is shown in figure B.3.

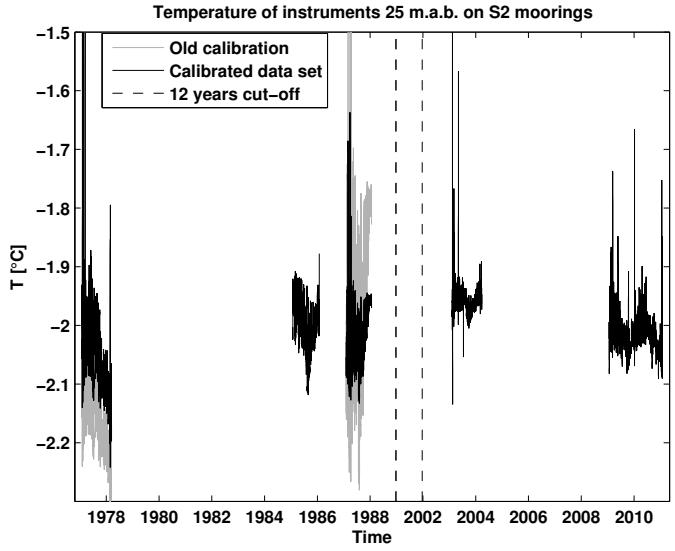

Figure B.3: The complete time series of bottom temperature at S2 with calibrated S2 1977 and 1987. The series are low-passed filtered with a 30 days cut-off to remove tidal oscillations. Note that a cut-off of 12 years have been done in the time series.

Appendix C

All data used at S2

Unfiltered data sets used from the S2 position are shown here, to illustrate the variability within the data. 14 days running means (black line) and 14 days low-passed filtered data (red line) have been included in all the temperature series (except fig. C.5). This is done to see the difference in the two smoothing procedures used in this investigation. The 2009 data are presented in figure C.5 with 14 days running means. The oxygen data from 2009 are presented together with the temperature and salinity series for the same year in figure C.5.

Two independently data sets for dissolved oxygen and conductivity at the S2 location in 2009 (see figure C.7 and C.6(a), respectively). Salinity data have been calculated for both conductivity data sets using a constant pressure of 602 dbars and the temperature series obtained from the the same year (see figure C.6(b)).

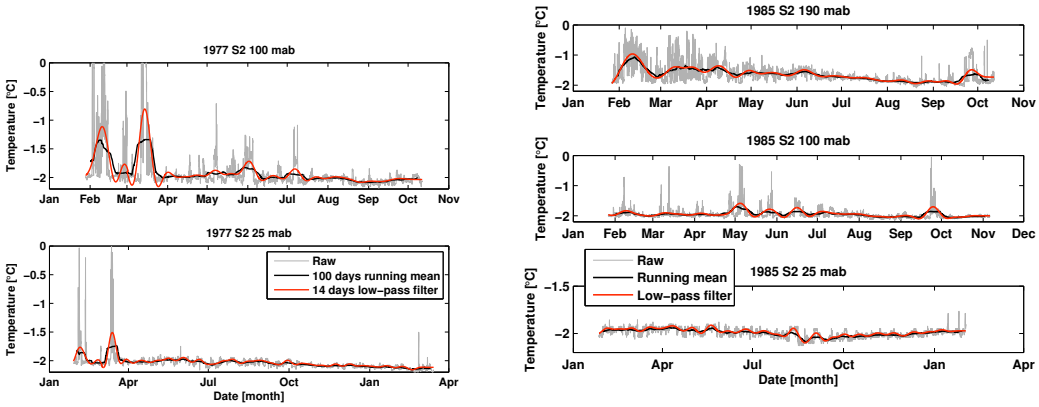

(a) 1977 (b) 1985

Figure C.1: Temperature series at all levels from a) S2 1977 and b) S2 1985.

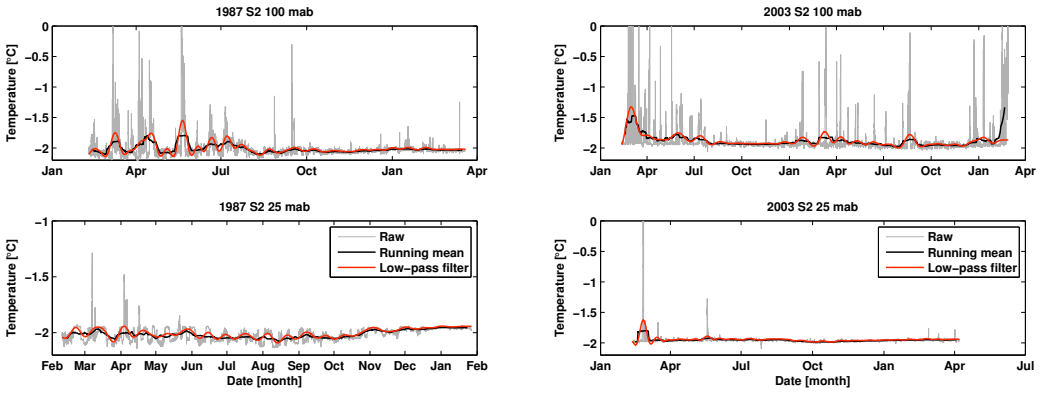

(a) 1987 (b) 2003

Figure C.2: Temperature series at all levels from a) S2 1987 and b) S2 2003.

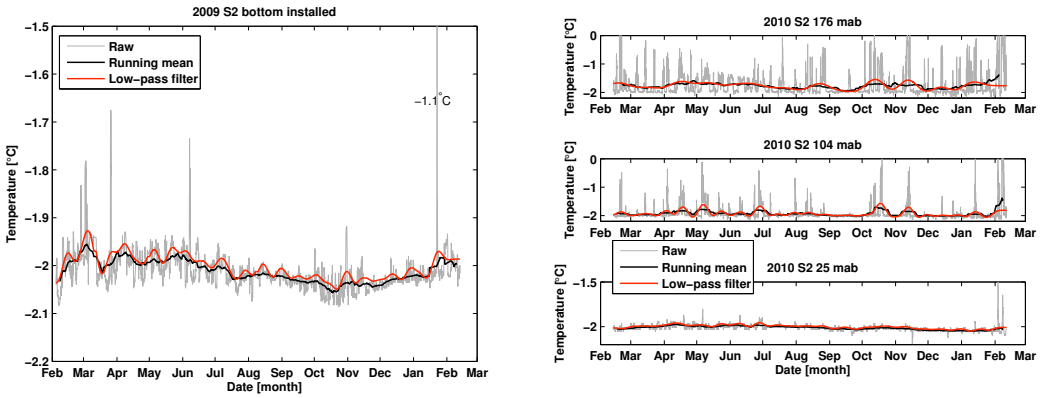

(a) Temp. 2009. (b) 2010

Figure C.3: Temperature series from sensors on RCMs from a) S2 2009 and b) S2 2010.

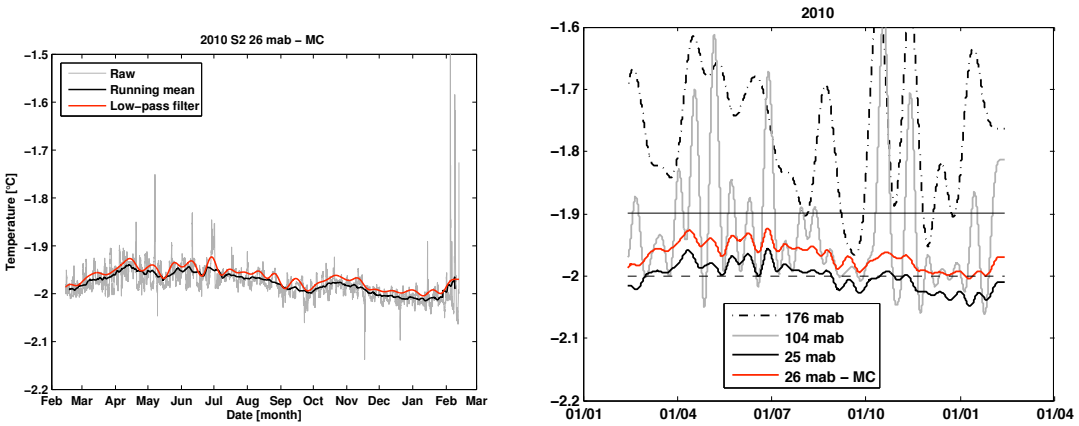

(a) 2010 MC

(b) Temp. from all instruments at the S2 2010.

Figure C.4: a) Temperature series from SBE-37 (Microcat) in 2010. 14 days running means (black line) and 14 days low-passed filtered data (red line) have been included. b) 14 low-passed filtered temperature data from all instruments included from the S2 mooring in 2010.

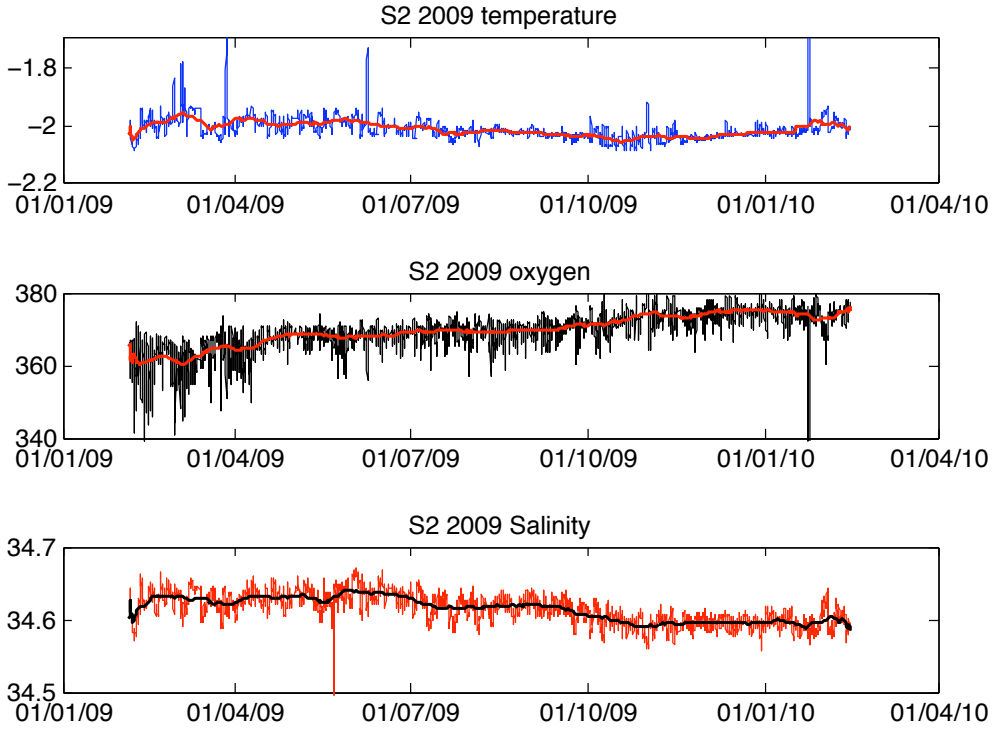

Figure C.5: Temp, oxygen and salinity data from 2009 with 14 days running means.

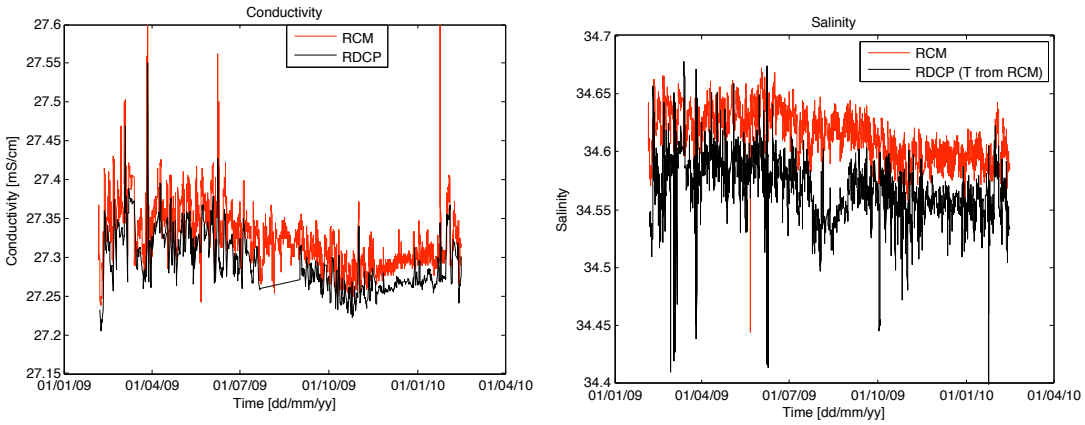

(a) Conductivity both RCM and RDCP 2009 (b) Salinity both RCM and RDCP 2009

Figure C.6: The RDCP salinities have been calculated using temperature from the RCM instrument and assuming a constant pressure at depth 602 m.

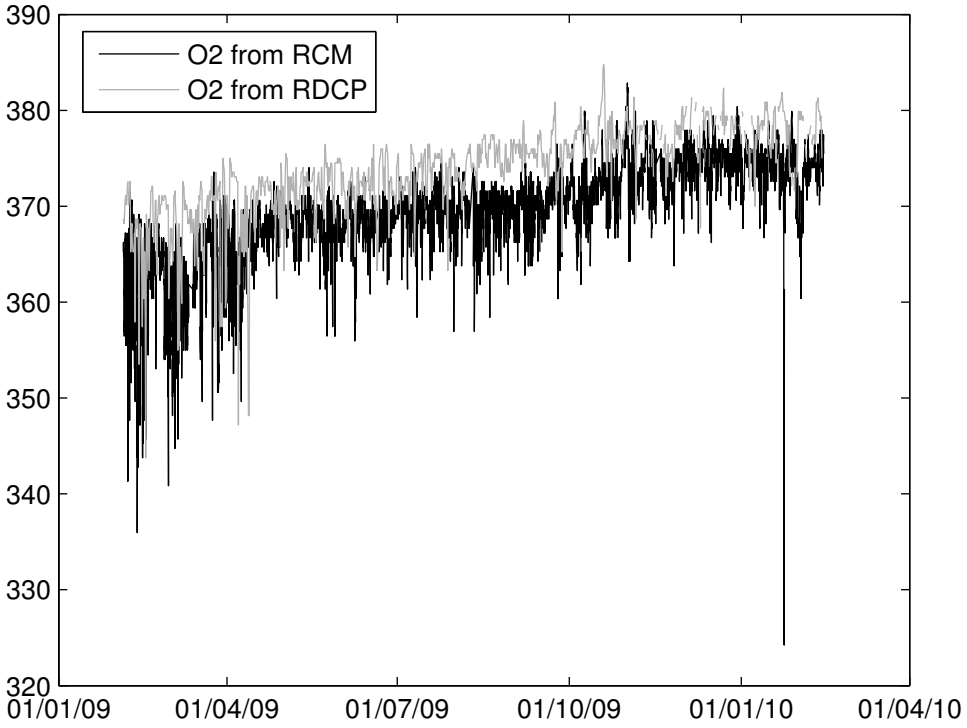

Figure C.7: The RDCP and RCM oxygen data of 2009.

Appendix D

Fast fourier transformation

Fast fourier transformation (FFT) has been used as an interpolation method for the regularly-spaced data set of monthly means at 25 m.a.b at S2. This has been done by estimating coefficients of a trigonometric polynomial fitting the 12 points. All six frequencies (max. amount of frequencies able to extract from a data set of 12 points) have been used, to represent as much of the signal as possible.

This type of interpolation of the given data set is done to make a smooth curve fitting the data, making a seasonal cycle for the ISW passing the S2 position.

The FFT was done on the monthly means of temperature. Figure D.1 show the different curves made. The green curve is made out of the monthly means from all years, while the black curve is made only with the monthly means containing more than 15 days of data. A clear difference is seen, and a further selection have been done, giving the thin grey curve. Here the data for 1985, 2009 and 2010 are used, assuming these years represent the climatic conditions. A figure with this curve superimposed on the monthly means are shown in figure D.2, to get an idea of how it fits the real data.

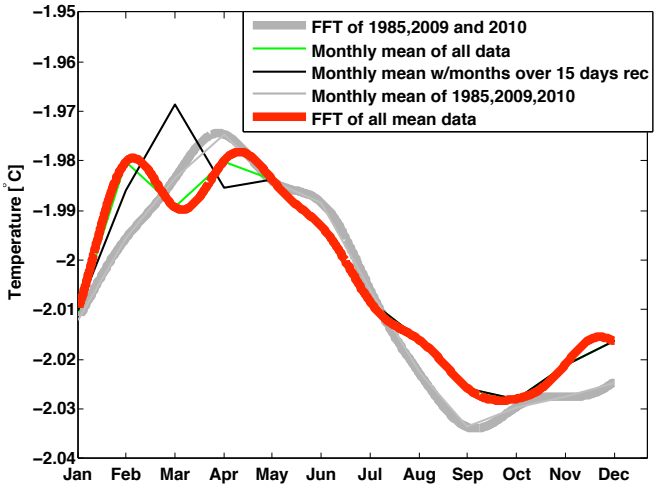

Figure D.1: The different curves made from the monthly means, see legend and text for explanation.

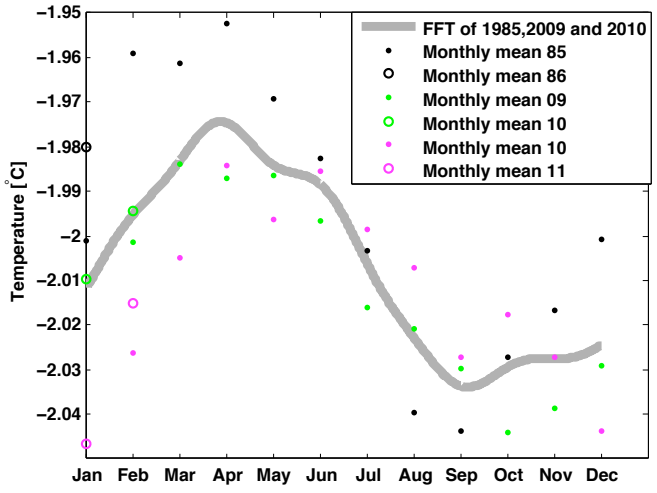

Figure D.2: The chosen FFT with the calculated monthly means from figure 5.6.

References

Brennecke, W., & Seewarte, D. 1921. *Die ozeanographischen Arbeiten der deutschen antarktischen Expedition 1911-1912*. Hammerich and Lesser.

Brown, E., & Bearman, G. 1999. *Seawater: its composition, properties and behaviour*. Butterworth-Heinemann.

Campbell, R.W. 1998. Filchner Ice Shelf, Antarctica: 1973, 1986. *Earthshots: Satellite Images of Environmental Change. U.S.*

Carmack, E.C. 1990. *Large-Scale Physical Oceanography of Polar Oceans*. Academic Press.

Carmack, E.C., & Foster, T.D. 1975b. Circulation and distribution of oceanographic properties near the Filchner Ice Shelf. *Deep Sea Research and Oceanographic Abstracts*, **22**, 77–90.

Colling, A. 2001. *Ocean circulation*. Elsevier.

Cushman-Roisin, B., & Beckers, J.M. 2009. *Introduction to geophysical fluid dynamics*. Academic Press.

Fahrbach, E., Hoppema, M., Rohardt, G., Schröder, M., & Wisotzki, A. 2004. Decadal-scale variations of water mass properties in the deep Weddell Sea. *Ocean dynamics*, **54**(1), 77–91.

Fofonoff, N.P., & Millard, R.C. 1983. *Algorithms for computation of fundamental properties of seawater*.

Foldvik, A., & Gammelsrød, T. 1988. Notes on Southern Ocean hydrography, sea-ice and bottom water formation. *Palaeogeography, Palaeoclimatology, Palaeoecology*, **67**(1-2), 3–17.

Foldvik, A., Gammelsrød, T., & Tørresen, T. 1985a. Hydrographic observations from the Weddell Sea during the Norwegian Antarctic Research Expedition 1976/1977. *Polar Research*, **3**, 177–193.

Foldvik, A., Gammelsrød, T., & Tørresen, T. 1985b. Physical oceanography studies in the Weddell Sea during the Norwegian antarctic Research Expedition 1978/79. *Polar Research*, **3**(2), 195–207.

Foldvik, A., Gammelsrød, Tor, Slotsvik, N., & Tørresen, T. 1985c. Oceanographic conditions on the Weddell Sea shelf during the German Antarctic Expedition 1979/80. *Polar Research*, **3**(2), 209–226.

Foldvik, A., Gammelsrød, T., & Tørresen, T. 1985d. Circulation and water masses on the southern Weddell Sea shelf. *Oceanology of the Antarctic Continental Shelf, Antarct. Res. Ser*, **43**, 5–20.

Foldvik, A., Gammelsrød, T., Nygaard, E., & Østerhus, S. 2001. Current measurements near Ronne Ice Shelf: Implications for circulation and melting. *Journal of geophysical research*, **106**(C3), 4463–4477.

Foldvik, A., Gammelsrød, T., Østerhus, S., Fahrbach, E., Rohardt, G., Schröder, M., Nicholls, K.W., Padman, L., & Woodgate, RA. 2004. Ice shelf water overflow and bottom water formation in the southern Weddell Sea. *Journal of geophysical research*, **109**(C2), C02015.

Foster, T.D., & Carmack, E.C. 1976. Frontal zone mixing and Antarctic Bottom Water formation in the southern Weddell Sea. *Deep Sea Research and Oceanographic Abstracts*, **23**, 301–317.

Gammelsrod, T., & Slotsvik, N. 1981. Hydrographic and current measurements in the southern Weddell Sea 1979/80. *Polarforschung*, **51**(1), 101–111.

Gammelsrød, T., Foldvik, A., Nøst, O.A., & Skagseth, O. 1994. Distribution of water masses on the continental shelf in the southern Weddell Sea. *Geophysical Monograph-American Geophysical Union*, **85**, 159–159.

Gill, A.E. 1973. Circulation and bottom water production in the Weddell Sea. *Deep Sea Research and Oceanographic Abstracts*, **20**, 111–140.

Gordon, A.L. 1982. Weddell deep water variability. *J. Mar. Res*, **40**, 199–217.

Gordon, A.L. 1998. Western Weddell sea thermohaline stratification. *Antarctic Research Series*, **75**, 215–240.

Grosfeld, K., Schröder, M., Fahrbach, E., Gerdes, R., & Mackensen, A. 2001. How iceberg calving and grounding change the circulation and hydrography in the

Filchner Ice Shelf-Ocean System. *Journal of Geophysical Research*, **106**(C5), 9039–9055.

http://lima.usgs.gov/. 2011. *Landsat Image Mosaic of Antarctica. U.S. Geological Survey.*

http://www.aadi.no/. 2011. *Aanderaa Data Instruments AS.*

http://www.bccr.no/BIAC/. 2011. *Bjerknes Centre for Climate Research. Bipolar Atlantic Thermohaline Circulation.*

http://www.gebco.net/. 2011. *General Bathymetric Chart of the Oceans.*

http://www.nsidc.org/sotc. 2011. *National Snow and Ice Data Center. State of the Cryosphere.*

http://www.seabird.com/. 2011. *Sea-Bird Electronics, Inc.*

Jacobs, S.S., Fairbanks, R.G., & Horibe, Y. 1985. Origin and evolution of water masses near the Antarctic continental margin: Evidence from H2 18O/H2 16O ratios in seawater. *Oceanology of the Antarctic Continental Shelf, Antarctic Res. Series*, **43**, 59–85.

Lambrecht, A., Sandhäger, H., Vaughan, D.G., & Mayer, C. 2007. New ice thickness maps of Filchner–Ronne Ice Shelf, Antarctica, with specific focus on grounding lines and marine ice. *Antarctic Science*, **19**(04), 521–532.

Lusquiños, A.J. 1963. *Extreme temperatures in the Weddell Sea.* Norwegian Universities Press.

Makinson, K., & Nicholls, K.W. 1999. Modeling tidal currents beneath Filchner-Ronne Ice Shelf and on the adjacent continental shelf: their effect on mixing and transport. *Journal of geophysical research*, **104**(C6), 13449–13.

Markus, T. 1996. The effect of the grounded tabular icebergs in front of Berkner Island on the Weddell Sea ice drift as seen from satellite passive microwave sensors. *Geoscience and Remote Sensing Symposium, 1996. IGARSS'96. Remote Sensing for a Sustainable Future, International*, **3**, 1791–1793.

Martinson, D.G., Killworth, P.D., & Gordon, A.L. 1981. A convective model for the Weddell Polynya. *J. Phys. Oceanogr*, **11**(4), 466–488.

McKee, D.C., Yuan, X., Gordon, A.L., Huber, B.A., & Dong, Z. 2011. Climate impact on interannual variability of Weddell Sea Bottom Water. *Journal of Geophysical Research*, **116**(C5), C05020.

Nicholls, K.W. 1996. Temperature variability beneath Ronne Ice Shelf, Antarctica, from thermistor cables. *Journal of geophysical research*, **101**(C1), 1199–1210.

Nicholls, K.W., & Østerhus, S. 2004. Interannual variability and ventilation timescales in the ocean cavity beneath Filchner-Ronne Ice Shelf, Antarctica. *Journal of geophysical research*, **109**, C04014.

Nicholls, K.W., Østerhus, S., Makinson, K., & Johnson, M.R. 2001. Oceanographic conditions south of Berkner Island, beneath Filchner-Ronne Ice Shelf, Antarctica. *Journal of geophysical research*, **106**(C6), 11481–11.

Nicholls, K.W., Padman, L., Schröder, M., Woodgate, R.A., Jenkins, A., & Østerhus, S. 2003. Water mass modification over the continental shelf north of Ronne Ice Shelf, Antarctica. *J. Geophys. Res*, **108**, 3260.

Nicholls, K.W., Østerhus, S., Makinson, K., Gammelsrød, T., & Fahrbach, E. 2009. Ice-ocean processes over the continental shelf of the southern Weddell Sea, Antarctica: A review. *Rev. Geophys*, **47**.

Nøst, O.A., & Østerhus, S. 1998. Impact of grounded icebergs on the hydrographic conditions near the Filchner Ice Shelf. *Ocean, Ice and Atmosphere: Interactions at the Antarctic Continental Margin, Antarct. Res. Ser*, **75**, 267–284.

Nowlin Jr., W.D., & Klinck, J.M. 1986. The physics of the Antarctic circumpolar current. *Reviews of geophysics*, **24**(3), 469–491.

Nygaard, E. 1994. *Transport av Isshelfvann i Weddellhavet.* M.Phil. thesis, Geophysical Institute, University of Bergen.

Pond, S., & Pickard, G.L. 2003. *Introductory dynamical oceanography.* Butterworth-Heinemann.

SeaBird Electronics, Inc. 2011 (March). *Conductivity and Temperature Recorder with RS-232 Interface SBE 37-SM MicroCAT.* 34 edn. SeaBird Electronics, Inc., 13431 NE 20 Street, Bellevue, Washington 98005 USA.

Weppernig, R., Schlosser, P., Khatiwala, S., & Fairbanks, R.G. 1996. Isotope data from Ice Station Weddell: Implications for deep water formation in the Weddell Sea. *Journal of Geophysical Research*, **101**, 25–25.